GEORG-AUGUST-UNIVERSITÄT
GÖTTINGEN

Fakultät für
Physik

Bachelor's Thesis

Studien von systematischen Unsicherheiten der im KLFitter genutzten Transferfunktionen zur Top-Quark-Rekonstruktion

Studies of Systematic Uncertainties of Transfer Functions used in the KLFitter for Top Quark Reconstruction

prepared by

Fritz Pasternok

from Nordhausen

at the II. Institute of Physics

Thesis number:	II.Physik-UniGö-BSc-2011/14
Thesis period:	4th April 2011 until 11th July 2011
First referee:	Prof. Dr. Arnulf Quadt
Second referee:	Prof. Dr. Johannes Haller

Zusammenfassung

Diese Bachelorarbeit stellt die Untersuchung der systematischen Unsicherheiten der im KLFitter genuttzen Transferfunktionen vor. Diese Untersuchung erfolgt durch die Einschränkung bestimmter Parameter bei der Berechnung der Transferfunktionen sowie die Verwendung unterschiedlicher Monte Carlo Samples und Objektdefinitionen. Es wird gezeigt, dass bestimmte Änderungen starken Einfluss auf die Transferfunktionen und andere keinen Einfluss auf eben diese haben. Die untersuchten Einflüsse sind das untere Ende des Energiefitbereichs, der maximale Abstand zwischen wahrem und rekonstruiertem Objekt, die Masse des Top Quarks, die maximal in einem Ereigniss zugelassene Zahl an Jets, der verwendete Zerfallskanal und die Anwendung eines Lebensdauertags für B-Jets. Zusätzlich wurde der Einfluss der Korrelationen der Parameter der Transferfunktion auf diese untersucht. Es wurde festgestellt, dass die Masse des Top Quarks auf alle Transferfunktionen geringen Einfluss hat ebenso wie der gewählte Zerfallskanal auf Transferfunktionen für Elektronen. Die Auswirkung der Anwendung eines Tags für B-Jets hat jedoch schwerwiegende Auswirkungen auf die Transferfunktionen.

Abstract

This bachelor thesis presents an investigation of the systematic uncertainties of the transfer functions used by KLFitter. This is done by applying cuts when calculating the transfer functions and using different Monte Carlo samples and object definitions. It is shown that there are certain modifications which have a strong influnce on the derived transfer functions as well as changes which keep the transfer functions stable. The investigated influences are the lower end of the energy range used for fitting, the maximum distance between truth object and reconstructed object, the top quark mass, the maximum allowed number of jets in an event, the decay channel used for transfer function calculation and the application of a b-jet lifetime tag. In addition the influence of the correlation of the transfer functions parameters on the uncertainties of the transfer functions has been investigated. The influence of the top quark mass for all transfer functions and the influence of the chosen decay channel for electron transfer functions were found to be negligible. The effect from the b-tag was found to be large.

Contents

1 Introduction

All currently observed particles and their interactions with the exception of gravity can be described by the Standard Model of particle physics. The latest particle of the Standard Model found in 1995 [1, 2] is the top quark. The top quark has some unique properties like its very short lifetime and its high mass. These facts and the one that it may be the link to new physics make studying it very interesting. Due to its high mass it cannot be produced at the existing lepton colliders and thus has to be produced at hadron colliders like the Large Hadron Collider and the Tevatron. The use of hadron colliders results in a large multijet background and due to the fact that only the partons of the hadrons interact the longitudinal component of the produced particles' momentum is unknown. This makes the reconstruction of top quark production events difficult. The decay channel used in analyses is often the semileptonic channel (see chapter 2.2.3) as it is a good compromise in terms of high branching ratio, low background and a clean signature. This channel has the disadvantage that it has a neutrino in its signature which's longitudinal momentum component can not be measured. Thus a fit has to be made. There are various approaches for $t\bar{t}$ reconstruction and fitting. One, the likelihood method, is applied by KLFitter. This approach requires transfer functions to translate the measured energy of the particles into the energy they actually had. These functions are derived from Monte Carlo samples. Monte Carlo samples can never describe the actual physical process 100% accurately and thus the influence of changing cuts and using different Monte Carlo samples on the derived transfer functions have been studied in this thesis.

2 Basics

2.1 The Standard Model

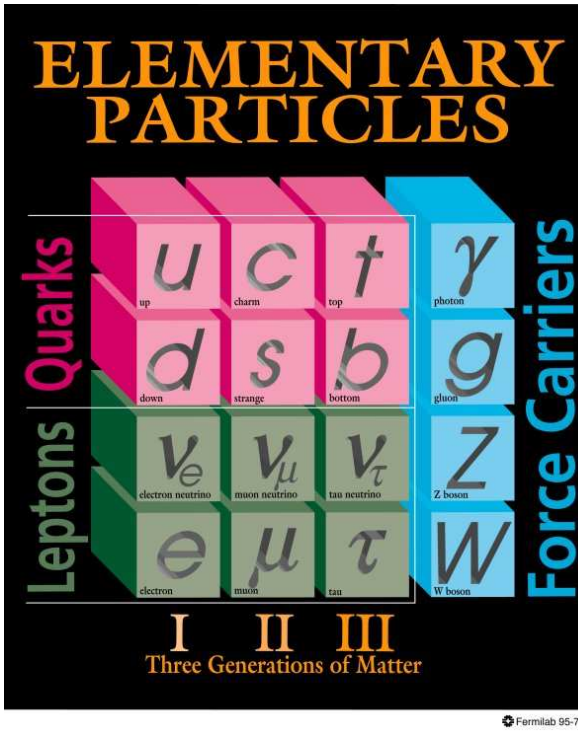

Figure 2.1: Particles of the Standard Model.

The Standard Model (SM) describes the elementary particles and their interactions. There are three types of elementary particles in the SM: quarks, leptons and gauge bosons. Quarks and leptons have spin $\frac{1}{2}$, the gauge bosons have spin 1 with exception of the Higgs particle which has spin 0.

There are two types of leptons: charged leptons and neutrinos. Charged leptons have mass and an electric charge of $-1e$. Neutrinos are neutral and almost massless. There

are also two types of quarks: up-type quarks and down-type quarks. The up-type quarks have an electric charge of $\frac{2}{3}$e, the down-type quarks of $-\frac{1}{3}$e. There are three generations of leptons and quarks. The higher generation's main difference to the lower ones is their increased mass. The leptons are from first to third generation the electron, the muon and the tauon and their respective neutrinos. Each of them has a lepton family quantum number. They are called electron number for the first, muon number for the second and tau number for the third generation. Both the neutrinos and their corresponding electron, muon or tauon have a value of 1 in their corresponding quantum number. There are also six antiparticles of these leptons. For these the electric charge and the family quantum number values change the sign.
Unlike the leptons the quarks do not have a single family quantum number for a generation. They have a quantum number for each of the three up-type and down-type quarks. The up-type quarks are from first to third generation: up, charm and top. The down-type quarks are down, strange and bottom. Their quantum number's names are identical to the names of the quarks. The down type quark's quantum number's value are -1 and the up-type's are $+1$. Quarks have an additional quantum number called colour. There are three colours: red, blue and green. For each quark one of these numbers is 1 while the others are 0. These numbers are not identical for all quarks of the same type. As there are antileptons there are also antiquarks with different sign in the electric charge and the quantum numbers mentioned above.
The gauge bosons are the photon for the electromagnetic interaction, the $W^{\pm}$ and the Z^0 for the weak interaction, eight gluons for the strong interaction and the Higgs particle which gives mass to all other particles. The photon, the Z, the gluons and the Higgs particle have an electric charge of 0e, the Ws of $\pm$1e. The photon and the Z couple to two leptons or two quarks of the same generation only. The gluons are the only gauge bosons which have colour. This allows them to couple to either two same generation quarks or to two or three other gluons. Each gluon carries one colour and one anticolour. The gluons preserve the colour quantums numbers when they couple. Like these the Ws couple to leptons of the same generation only but the Ws can couple to two quarks of different generations. These couplings over generations are suppressed and are described by the Cabibbo-Kobajashi-Maskawa(CKM)-matrix (2.1, [3]). The Higgs boson is the only SM particle which has not been found yet.

$$V_{CKM} = \begin{pmatrix} 0.97428 \pm 0.00015 & 0.2253 \pm 0.0007 & 0.00347^{+0.00016}_{-0.00012} \\ 0.2252 \pm 0.0007 & 0.97345^{+0.00015}_{-0.00016} & 0.0410^{+0.0011}_{-0.0007} \\ 0.00862^{+0.00026}_{-0.00020} & 0.0403^{+0.0011}_{-0.0007} & 0.999152^{+0.000030}_{-0.000045} \end{pmatrix} \tag{2.1}$$

2.2 The Top Quark

The top quark is the heaviest fermion in the SM. The current world average of its mass is $172.0 \pm 0.9 \pm 1.3 \ \frac{\text{GeV}}{c^2}$ [3], making it more than 30 times heavier than the second heaviest fermion, the bottom quark, with $4.19^{+0.18}_{-0.06} \ \frac{\text{GeV}}{c^2}$ [3]. The SM predicts the top quark's charge to be $+\frac{2}{3}e$. However this has not been measured in electromagnetic production of the top quark. Its lifetime is $5 \cdot 10^{-25}$ s. This is about 100 times smaller than the time necessary for hadronisation. Because of this the top quark passes its spin information on to its decay products.
The top quark's high mass might offer insights into new physics, e.g. couplings to the Higgs boson are expected to be mass dependent, leading to a high cross section for the coupling of the Higgs boson to the top quark.

2.2.1 $t\bar{t}$ production

One way to produce top quarks is via strong coupling in $t\bar{t}$-production. There are four leading order Feynman diagrams for production via the strong interaction which contribute to this process.

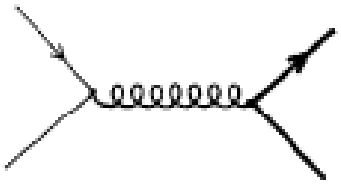

Figure 2.2: Feynman diagram for top quark production via $q\bar{q}$ annihilation [4].

The first one is quark antiquark annihilation shown in figure 2.2.

The other three are shown in figure 2.3. In these cases the top quark pair is produced via fusion of two gluons.
At the LHC (see chapter 2.3) the cross section for gluon-gluon-fusion is much larger than for q-qbar-annihilation. This results from the parton distribution functions shown in

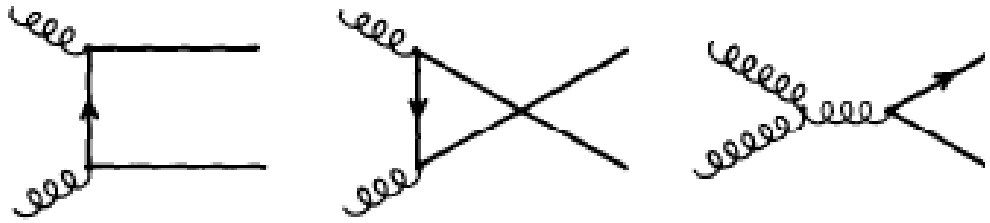

Figure 2.3: Feynman diagram for top quark production via gluon gluon fusion [4].

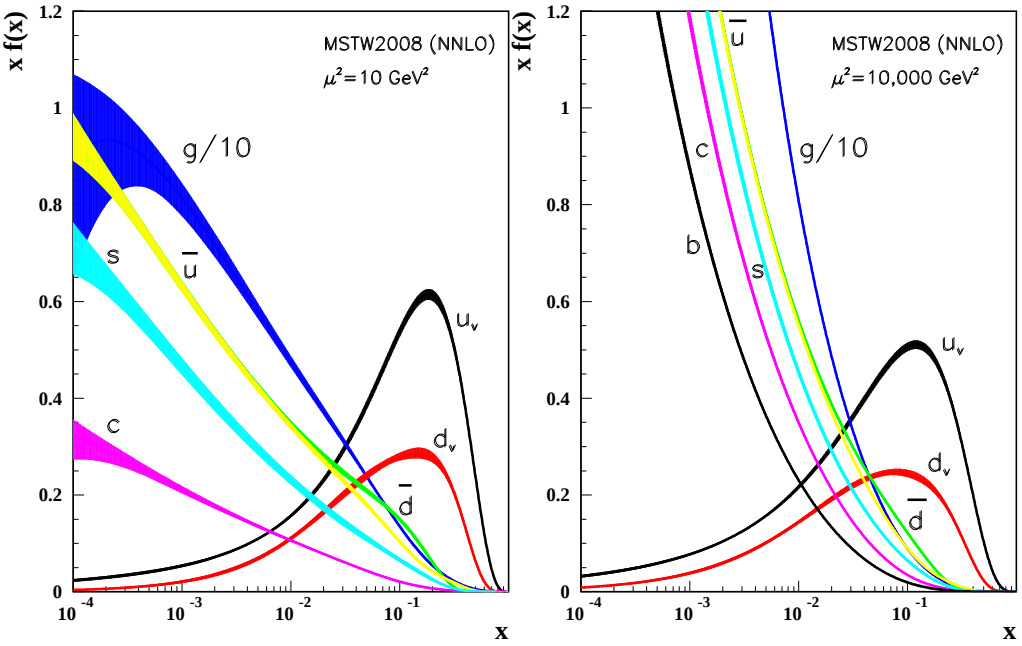

Figure 2.4: Parton distribution functions $f(x)$ [3].

figure 2.4. The required fraction of the proton's momentum for $t\bar{t}$ production becomes lower with higher centre of mass energy. For low values of this fraction the ammount of gluons having at least that much energy grows greatly while the ammount of quarks with enough energy grows only slightly. Thus the $q\bar{q}$ annihilation was the dominant process at the Tevatron but at the LHC the dominant process is gluon gluon fusion.

2.2.2 Single Top Production

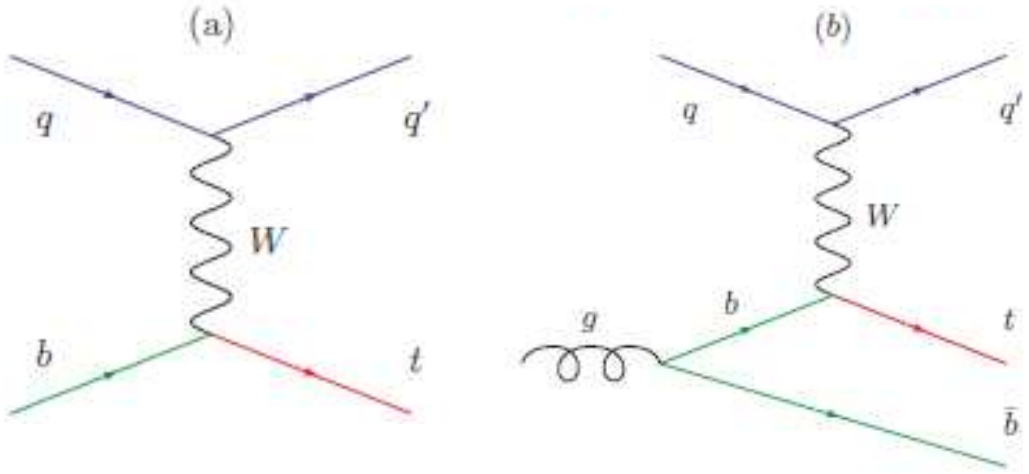

Figure 2.5: Feynman diagrams for the single top quark production [5].

The main process for single top production is the interaction of a W boson with a bottom quark. This process creates in almost 100% of the cases a top quark because the CKM-matrix elements for the other processes are very close to zero. The bottom quark of this process is usually created via QCD processes. Figure 2.5 shows the Feynman diagram of this process. Since the top quark is produced from a W boson, the cross section is a function of the top quark's electric charge. This can be used to calculate the top quark's charge if the cross section can be measured with sufficiently high precision. But the single top quark production's cross section is low compared to the $t\bar{t}$ production's cross section and thus it is just a background for $t\bar{t}$ analyses.

2.2.3 Decay

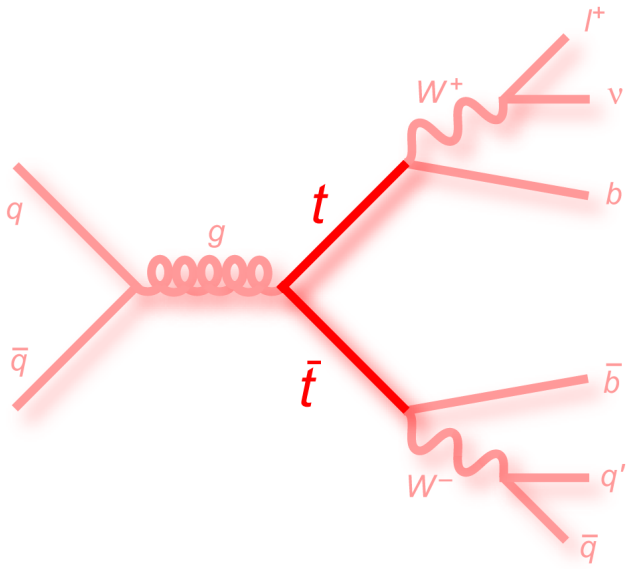

Figure 2.6: Feynman diagram for a $t\bar{t}$ decay in the semileptonic channel.

The top quark decays in almost 100% of the cases into a W-boson and a bottom quark. The W-boson can then decay either hadronically into a quark and an antiquark or leptonically into a lepton and a neutrino. Based on this, there are three channels a top-antitop-pair can decay into: the full hadronic channel where both Ws decay hadronically, the dileptonic channel where both Ws decay leptonically and the semileptonic channel where one W decays hadronically and one leptonically. The leading order Feynman diagram for the semileptonic channel is shown in figure 2.6.
The full hadronic channel has the highest cross section of these three channels but also a high QCD background which makes the reconstruction of the $t\bar{t}$-decay difficult. The dileptonic channel has the lowest cross section but also the lowest background, but the two neutrinos lead to high missing transverse energy and make the event reconstruction difficult because it is not clear to which neutrino which amount of missing transverse energy belongs. The semileptonic channel has moderate cross section and its signature is not as clear as for the dileptonic channel but can be separated from background more easily than the full hadronic signature, making it the best choice of the three channels for most measurements.
The two bottom quarks from the $t\bar{t}$-decay are measured as jets. These jets have high transverse energy and come usually from a secondary vertex due to the b quarks long life-

time. They can be separated from light jets using b-tagging for example via a secondary vertex technique.

2.3 LHC

The Large Hadron Collider (LHC) is a proton-proton collider located at CERN in Geneva. The LHC is designed to reach centre of mass energies of 14 TeV with a peak luminosity of 10^{34} cm^{-2}s^{-1} [7]. The desired centre of mass energies cannot been reached without great efford with a synchrotron type lepton-lepton collider since the energy loss due to synchrotron radiation, which is proportional to E^4, would cause energy losses too high to be compensated. Thus the LHC is a hadron collider as energy loss due to synchrotron radiation is proportional to m^{-4}. Reaching luminosities of 10^{34} cm^{-2}s^{-1} is not possible with a proton-antiproton collider due to the difficulties of producing antiprotons at sufficiently high rate. Thus it is a proton-proton collider and has two rings with a lenght of 26.7 km [7] which contributes to the reduction of the energy loss due to synchrotron radiation as it is proportional to r^{-1}. The tunnel used for the LHC was initially constructed for the LEP accelerator, but is used for the LHC since the shutdown of LEP.

2.3.1 ATLAS

ATLAS is one of the experiments at the LHC. The ATLAS detector is an general-purpose-dectector. It is shown schematically in figure 2.7. In its centre is the tracking detector which consists of a high resolution pixel detector, a silicon microstrip tracker and a transition radiation tracker. The pixel detector has on a surface of 1.7 m^2 80 million channels resulting in a spatial resolution at the order of μm. In this part of the detector a superconducting solenoid magnet creates a magnetic field of 2 T in order to bend the tracks of charged particles. The radius of the particles' curves can then be used to determine their electric charge. This part of the detector is followed by a liquid argon electromagnetic calorimeter. This is surrounded by the hadronic calorimeter which is a tile calorimeter with exception of the liquid argon endcaps. The last part of the detector is the muon system. It consists of thin-gas-chambers, resistive-plate-chambers, monitored-drift-tubes and cathode-strip-chambers. In the muon system a toroid magnet creates a 4 T magnetic field to bend the trajectories of the muons.
With a lenght of 44 m and a diameter of 25 m ATLAS is the largest detector at the LHC. But its mass of 7000 t is surpassed by the CMS detector.
At design luminosity about 40 million bunches of 100 billion particles pass through it each second. This leads to about a billion collisions per second. To be able to get as much

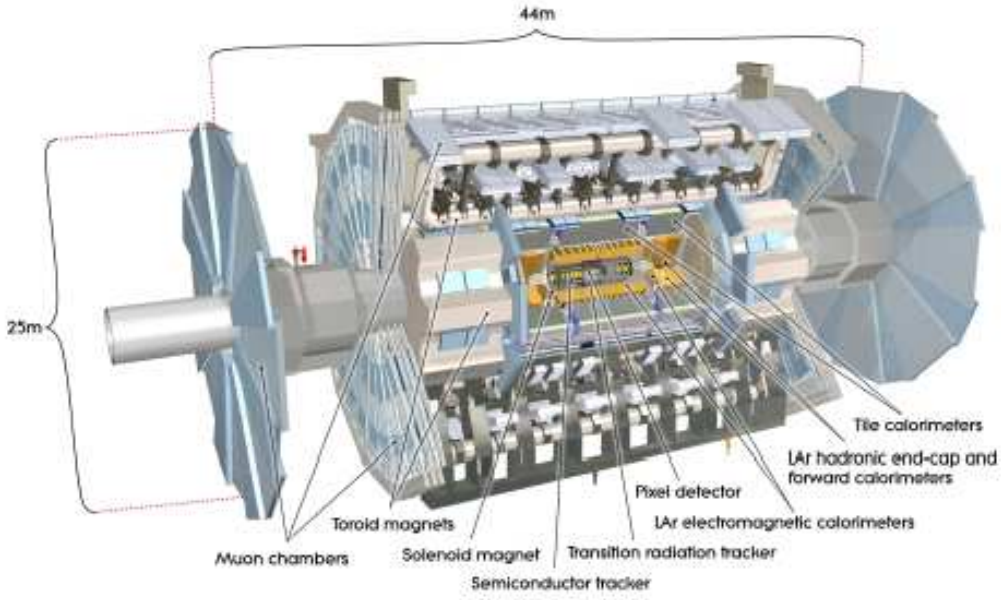

Figure 2.7: The ATLAS detector [6].

data from these events as possible, ATLAS uses a three level trigger system. This system decreases the rate of data by a factor of 200000 to about 320 MB per second.

3 $\mathrm{t\bar{t}}$ Reconstruction

3.1 KLFitter

The Kinematic Likelihood Fitter (KLFitter) is a programme which reconstructs top-antitop-decays. It fits a given event to a kinematic model using a likelihood function L. First the likelihood is calculated for all permutations of the particles, because it is unknown which jet was created from which top quark or W boson. Then the likelihoods are maximised via variation of its parameters including the energy of the jets and leptons. During this maximisation boundary conditions are taken into account. E.g. the further of the mass of the two jets combined to the W is from the W mass the lower will be the likelihood. In the end the fitter returns the best fit parameters and the corresponding value of the likelihood as well as relative weight for all permutations.

$$L = \left(\prod_{i=1}^{4} W(\tilde{E}_i, E_i)\right) \cdot W(\tilde{E}_l, E_l) \cdot W(E_x^{miss}|p_x^{\nu}) \cdot W(E_y^{miss}|p_y^{\nu}) \cdot \left(\prod_{i=1}^{4} W(\tilde{\Omega}_i, \Omega_i)\right) \cdot BW(m_{jj}|M_W) \cdot BW(m_{e\nu}|M_W) \cdot BW(m_{jjj}|M_{top}) \cdot BW(m_{e\nu j}|M_{top}) \tag{3.1}$$

Equation 3.1 [8] shows the likelihood function used by KLFitter. $BW(x|y)$ are Breit-Wigner functions centered around y, $W(E_{x/y}^{miss}|p_{x/y}^{\nu})$ the transfer function (see chapter 3.2) of the neutrino momentum, $W(\tilde{E}, E)$ the transfer functions of the quarks and leptons and $W(\tilde{\Omega}, \Omega) = W(\tilde{\eta}, \eta) \cdot W(\tilde{\phi}, \phi)$ the transfer functions of all quark angles.

3.2 Transfer Functions

KLFitter allows to check if a kinematic model describes the data gathered with the ATLAS detector, but the kinematic model does not describe inefficiencies and losses from the detector as well as disturbances from exterior sources. To take these into account the energies or momenta of the jets and particles are adjusted using transfer functions. So

transfer functions translate the measured particle at detector level into the true particle at parton level. To obtain the transfer functions Monte Carlo samples describing both the particle at parton level and the particle at detector level are used.

3.3 TFTool

TFTool is an application to calculate transfer functions for specific particle types from Monte Carlo samples (MC samples). The transfer functions are in this case the relative difference ΔE between the reconstructed energy of the particle E_{reco} and its true energy E_{truth} to its true energy.

$$\Delta E = \frac{E_{truth} - E_{reco}}{E_{truth}}$$

The first step for the calculation is to identify the objects in the MC samples. Then the truth and reconstructed objects are matched to each other. This process is called matching. In case multiple reconstructed objects are matched to a single truth object or the other way round, these objects are removed. Additionally overlapping objects with too small a distance dR are removed from the event.

$$dR = \sqrt{(\phi_1 - \phi_2)^2 + (\eta_1 - \eta_2)^2} \tag{3.2}$$

Then ΔE is calculated for all remaining objects and written into histograms.
The best currently known way to describe the resulting histograms via a function is the sum of two Gauss functions. This function is called double Gauss function. Assuming that the parameters of the double Gauss function are independent of the energy, the double Gauss function describes the transfer function well only for a specific energy. To compensate for this the parameters of the double Gauss function are chosen to be energy dependant. These parameters are the mean values (mean_1 & mean_2) and width (width_1 & width_2) of both Gauss functions and the size of the second Gauss relative to the first (scale). The energy dependance of these parameters is assumed linear except a better description is known. For example this is the case for the width of the primary Gauss of calorimeter objects where the dependance is $\frac{a}{\sqrt{E_{truth}}} + b$ with parameters a and b. This choice is made for calorimeter objects because the calorimeter resolution is proportional to $\frac{1}{\sqrt{E}}$. The muon systems resolution is proportinal to p_T. Thus linear functions in p_T are the functions of choice for the muons primary Gauss width. To prevent the parameters to produce unphysical results, the parameters are restricted to specific regions of values.

parton type	mean_1(p_0)	width_1(p_1)	scale(p_2)	mean_2(p_3)	width_2(p_4)
b-jets	$\frac{a}{E_{truth}} + b \cdot E_{truth}$	$\frac{c}{E_{truth}} + d$	$\frac{e}{E_{truth}} + f \cdot E_{truth}$	$g + h \cdot E_{truth}$	$i + j \cdot E_{truth}$
light jets	$a + b \cdot E_{truth}$	$\frac{c}{E_{truth}} + d$	$e + f \cdot E_{truth}$	$g + h \cdot E_{truth}$	$i + j \cdot E_{truth}$
electrons	$a + b \cdot E_{truth}$	$\frac{c}{E_{truth}} + d$	$e + f \cdot E_{truth}$	$g + h \cdot E_{truth}$	$i + j \cdot E_{truth}$
muons	$a + b \cdot E_{truth}$	$c + d \cdot E_{truth}$	$e + f \cdot E_{truth}$	$g + h \cdot E_{truth}$	$i + j \cdot E_{truth}$

Table 3.1: Functions used to decscribe the energy dependance of the parameters. The names in brackets are the names of the parameters used in the figures.

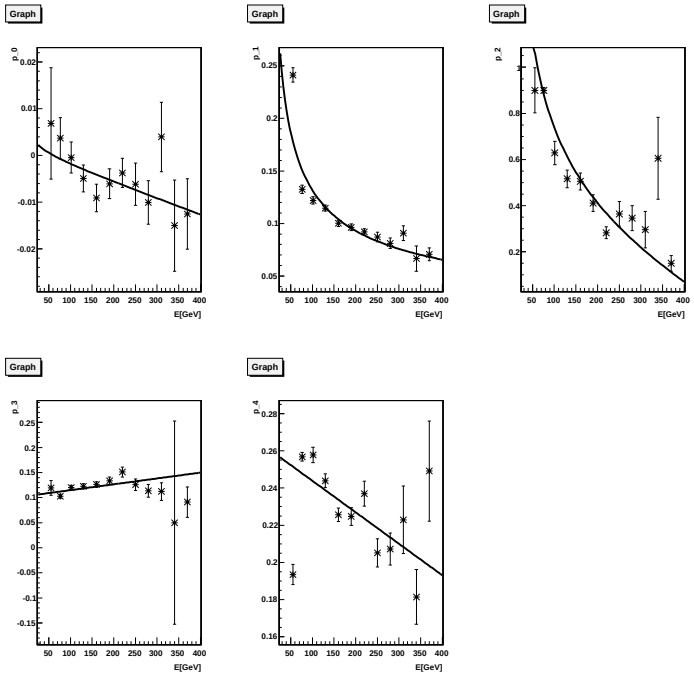

Figure 3.1: Functions fitted to the parameters for b-jets.

The functions used to fit these parameters can be found in table 3.1. The figures 3.1, 3.2 and 3.3 show fits to the parameters using these functions.

These 10 parameters are correlated. This correlation is required for the correct calculation of the uncertainties of the transfer functions and has to be extracted during the fitting process. Figure 3.4 shows an example for these correlations.

$$W = \frac{1}{2 \cdot \pi} \cdot \frac{1}{\text{width}_1 + \text{scale} \cdot \text{width}_2} \cdot \left(e^{-\frac{(\Delta E - \text{mean}_1)^2}{2 \cdot \text{width}_1{}^2}} + \text{scale} \cdot e^{-\frac{(\Delta E - \text{mean}_2)^2}{2 \cdot \text{width}_2{}^2}} \right) \tag{3.3}$$

The actual fitting process is done in two steps. First an energy independant double

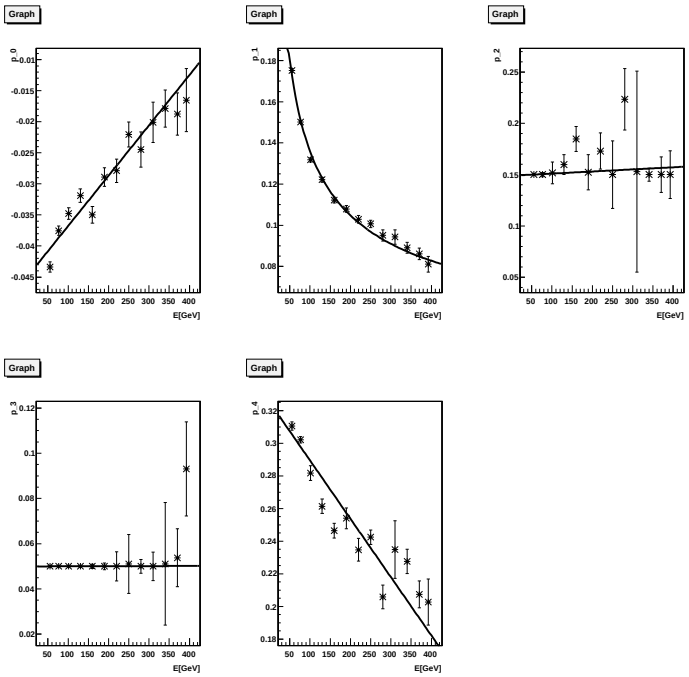

Figure 3.2: Functions fitted to the parameters for light jets and electrons. p_3 is at its lower limit.

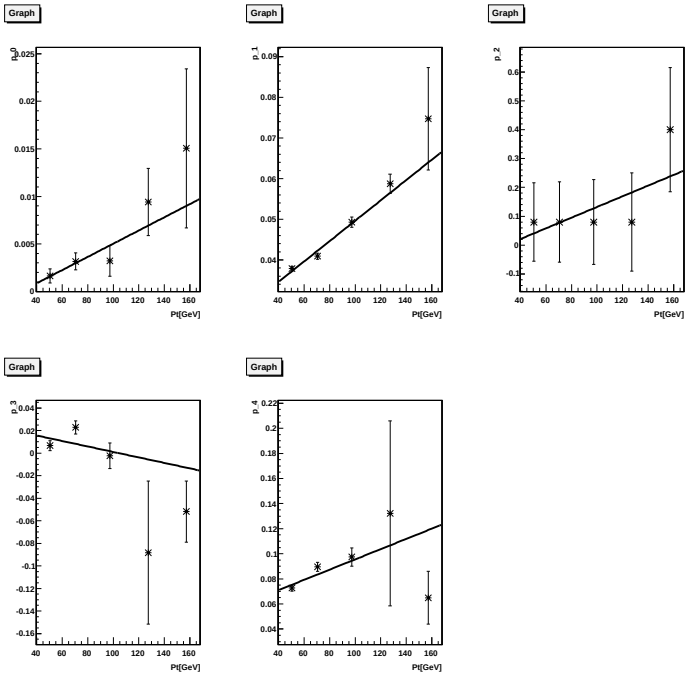

Figure 3.3: Functions fitted to the parameters for muons.

Gauss function is fitted to the histograms (local fit). This is done for different truth

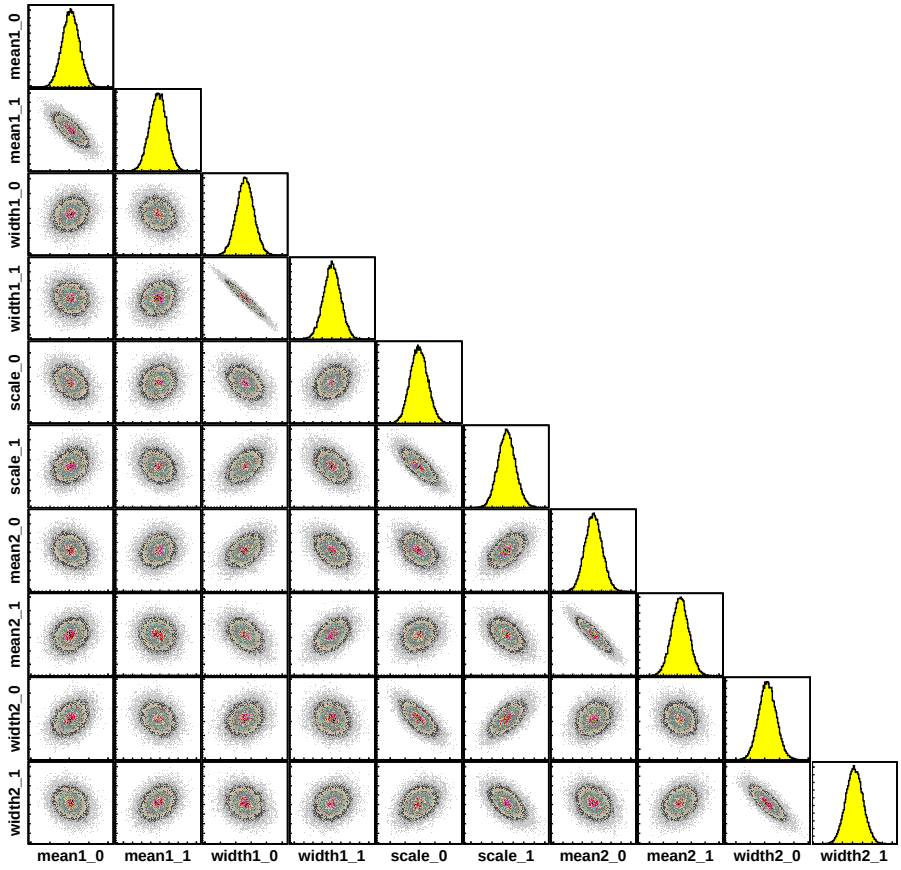

Figure 3.4: Correlation of the parameters of the MC10b light jet transfer function in the eta region $|\eta| \in [0; 0.8]$ calculated by TFTool.

energies. The parameters of these double Gauss functions are then used as starting values for fitting an energy dependant double Gauss to the histograms (global fit). The function of the double Gauss is shown in equation 3.3.

4 Performed Tests

Two datasets have been used for the following analysis: Moriond_TP_16.0.3.3.3_GTT_02-01-05 for the fit range, matching radius and top mass analyses, MC10b for the jet multiplicity, leptonic channel and b-tag analyses.
In order to study the systematic uncertainties of transfer functions used in KLFitter the following tests have been performed.

4.1 Fit Range

The parameters for low energies from the local fits have a large uncertainty and tend to be far off from the function fitted to the parameters for high energies. This would increase the uncertainties of the transfer functions and thus TFTool does not use parameters below a specific energy for the global fit. It was tested how much this energy cut E_{min} affects the transfer functions. The cut was 110 GeV for jets and 50 GeV for leptons. It was lowered to 50 GeV for jets and 20 GeV for leptons.

4.2 Matching Radius

The matching radius is the highest allowed distance dR_{max} (see equation 3.2) from the truth object to the reconstructed one. Until now quite a high value of $dR_{max} = 0.3$ has been used. To test its influence on the transfer functions, transfer functions for $dR_{max} = 0.30$, $dR_{max} = 0.10$ and $dR_{max} = 0.05$ have been calculated with all other parameters fixed.

4.3 Top Mass

There are MC samples available for different top masses. It was checked what influence the choice of MC samples for different top masses has on the transfer functions. The masses used are 160 $\frac{\text{GeV}}{c^2}$, 175 $\frac{\text{GeV}}{c^2}$, and 190 $\frac{\text{GeV}}{c^2}$.

4.4 Parameter Correlation

The parameters of the double Gauss function are correlated as metioned in chapter 3.3. To extract the correlation coefficients the TFTool source code had to be adjusted. Because of that this correlation was not taken into account when calculating the uncertainties for the fit range, matching radius and top mass analysis. The correlations are taken into account for the jet multiplicity analysis and the transfer functions for the MC10b dataset.

4.5 Jet Multiplicity

There can be a varying number of jets per event. A high number of jets can make the reconstruction more difficult. Thus, the influence of the jet multiplicity on the transfer functions was investigated. The number of jets in an event was used as a cut. This cut was set to four, six and eight, and the transfer functions calculated from this were compared to transfer functions without this cut.

4.6 Event Topology

MC samples contain events for the semileptonic and the dileptonic decay channels. It was investigated if the different topology between these two decay channels has an influence on the derived transfer functions. If not, statistics could be improved by using both samples together for the calculation of the transfer functions. Also, analyses on both channels could make use of the same set of transfer functions.

4.7 B-tag

B-jets can be tagged using different methods. It has been investigated, if requiring a lifetime tag has an effect on the transfer functions.

4.8 Calculation and Uncertainties

The transfer functions shown in chapter 5 have been calculated from the equation 3.3 using the parameters delivered by TFTool.

$$\sigma_W^2 = \sum_{\alpha=a}^{j} \left(\left(\frac{\mathrm{d}W}{\mathrm{d}\alpha} \right)^2 \cdot \sigma_\alpha^2 \right) + \sum_{\beta=a}^{j} \left(\sum_{\gamma=a;\gamma\neq\beta}^{j} \left(\frac{\mathrm{d}W}{\mathrm{d}\beta} \cdot \frac{\mathrm{d}W}{\mathrm{d}\gamma} \cdot C_{\beta\gamma} \cdot \sigma_\beta \cdot \sigma_\gamma \right) \right) \tag{4.1}$$

The uncertainties σ_W of the transfer functions are calculated using the equation 4.1 where $C_{\beta\gamma}$ is the correlation coefficient of the parameters β and γ. The uncertainties of the parameters a to j are delivered by TFTool as well as the correlation coefficients. For the analyses where the correlation coefficients were not available they were set to 0.

$$\sigma_{dW}^2 = \sigma_{W_1}^2 + \sigma_{W_2}^2 \tag{4.2}$$

The uncertainties σ_{dW} of the difference dW of transfer functions W_1 and W_2 are calculated using the equation 4.2.

5 Results

In this chapter natural units will be used ($c = 1$). Thus masses are not given in $\frac{\text{GeV}}{\text{c}^2}$ but in GeV.

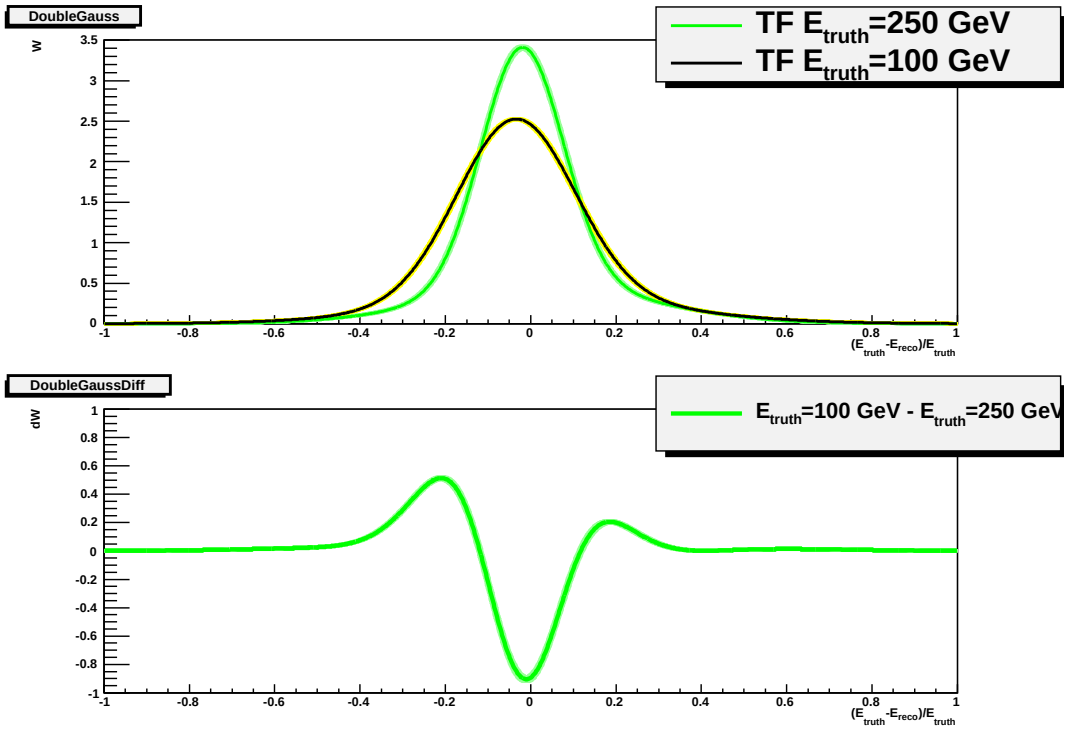

Figure 5.1: Transfer functions for MC10b light jets in the eta region $|\eta| \in [0; 0.8]$. The upper plot shows the transfer functions using the parameters shown in the legend. The lower plot shows the difference of these transfer functions as shown in the legend.

The figures 5.1 and 5.2 show the transfer functions for light jets for the energies $E_{truth} =$ 100 GeV and $E_{truth} = 250$ GeV in the eta ranges from 0.00 to 0.80 and 1.52 to 2.50. The MC10b samples have been used to calculate these transfer functions. The functions for the same eta region differ for different energies as metioned in chaper 3.3.

The figures 5.3, 5.4, 5.5 and 5.6 show this for b-jets and electrons.

Shown in the figures 5.7 and 5.8 is this for muons. Unlike the other partons the muon transfer functions width increases greatly with the energy, because its width is

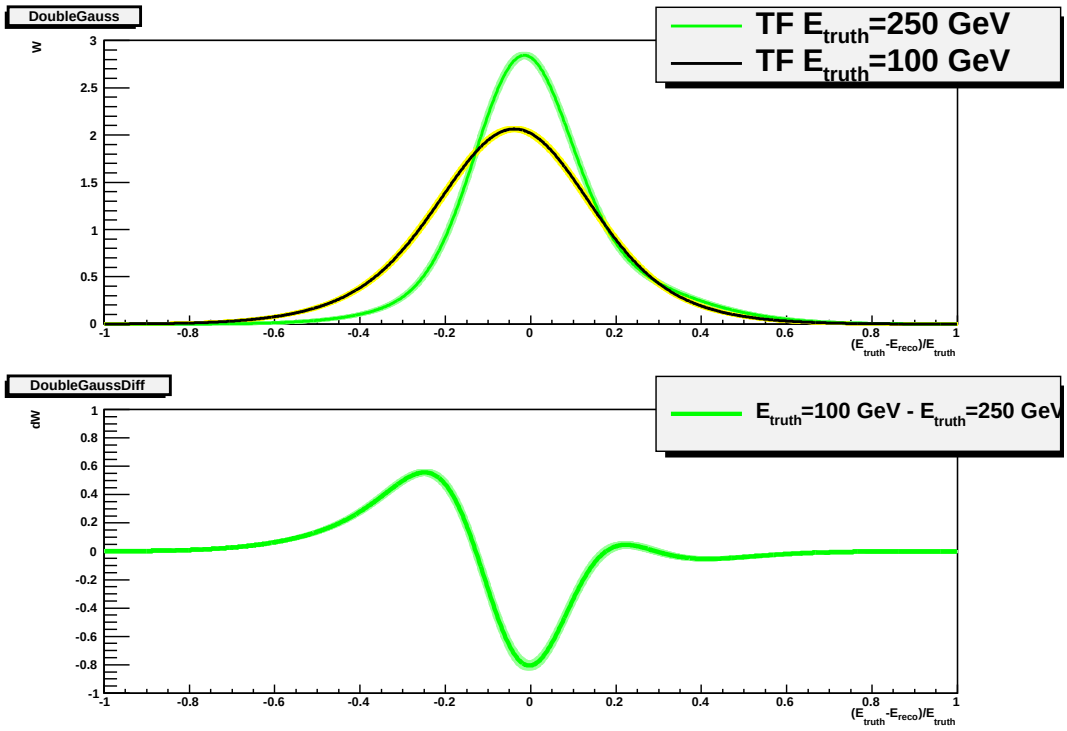

Figure 5.2: Transfer functions for MC10b light jets in the eta region $|\eta| \in [1.52; 2.5]$.

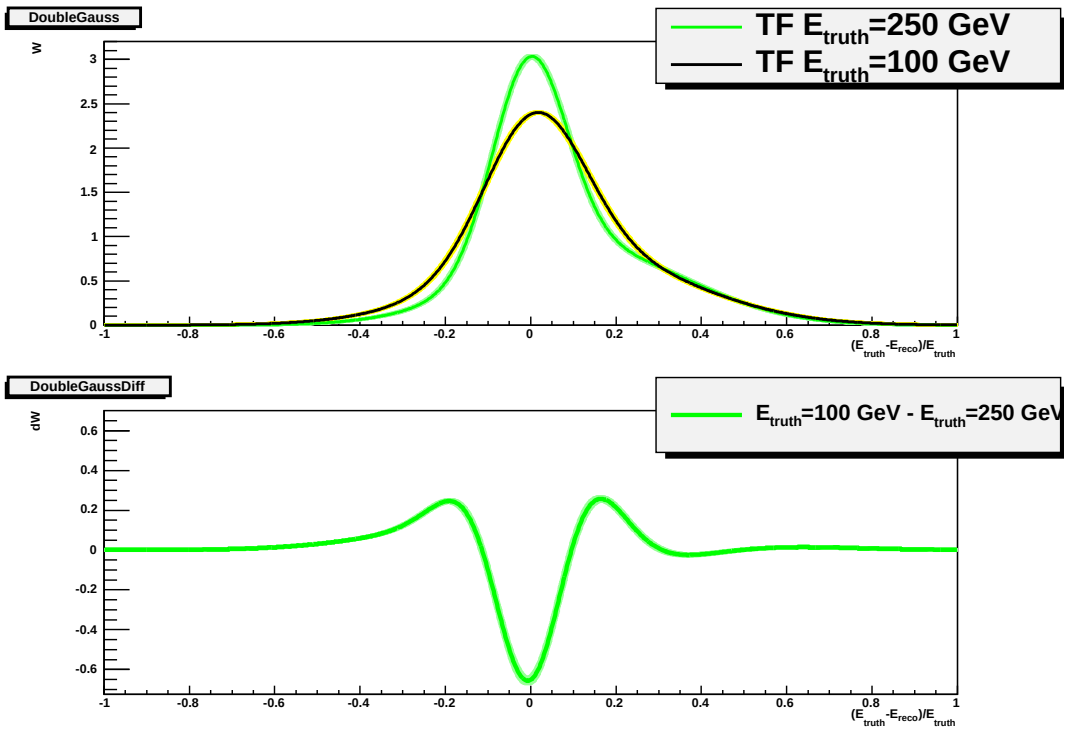

Figure 5.3: Transfer functions for MC10b b-jets in the eta region $|\eta| \in [0; 0.8]$.

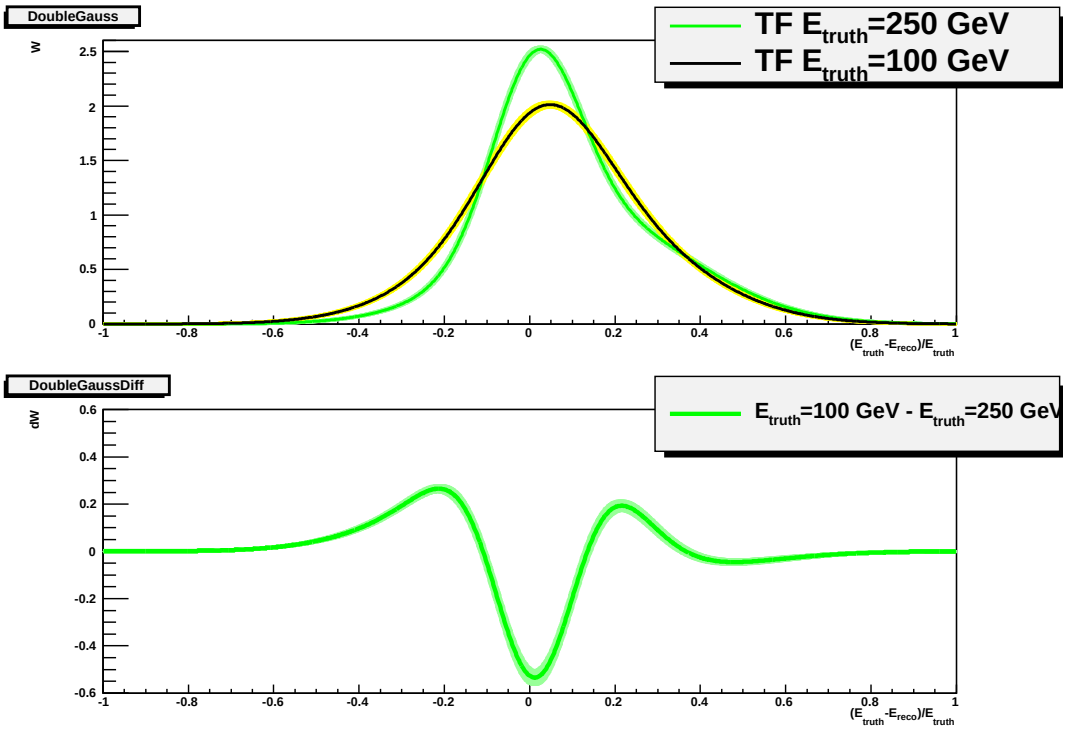

Figure 5.4: Transfer functions for MC10b b-jets in the eta region $|\eta| \in [1.52; 2.5]$.

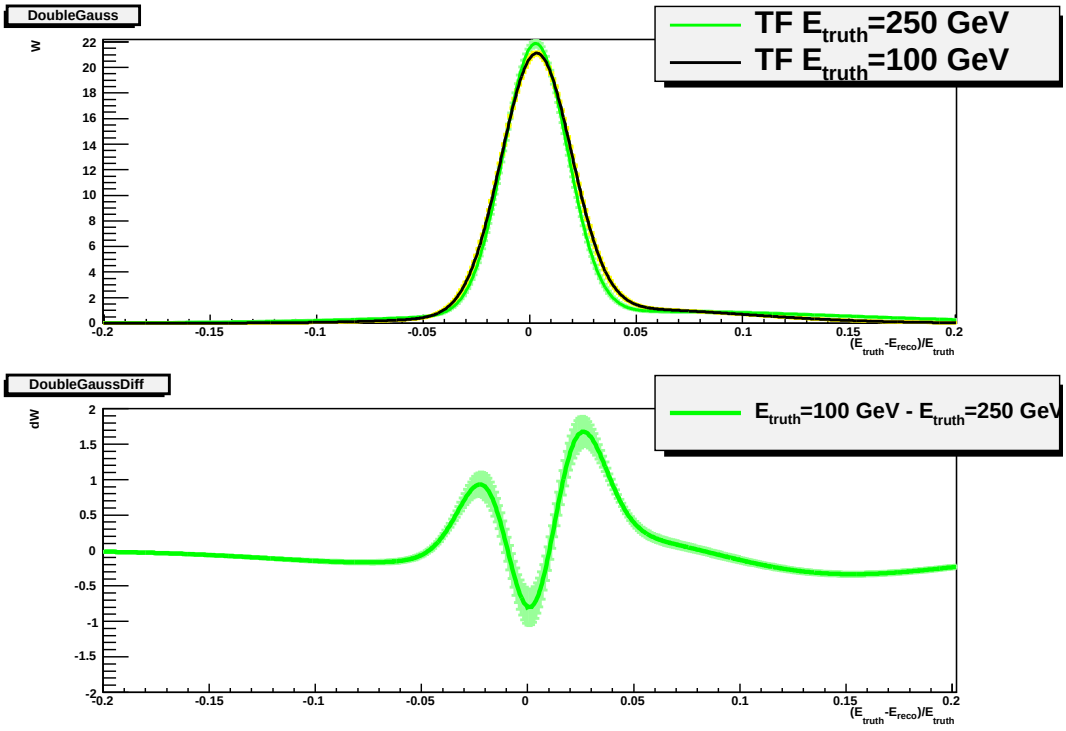

Figure 5.5: Transfer functions for MC10b electrons in the eta region $|\eta| \in [0; 0.8]$.

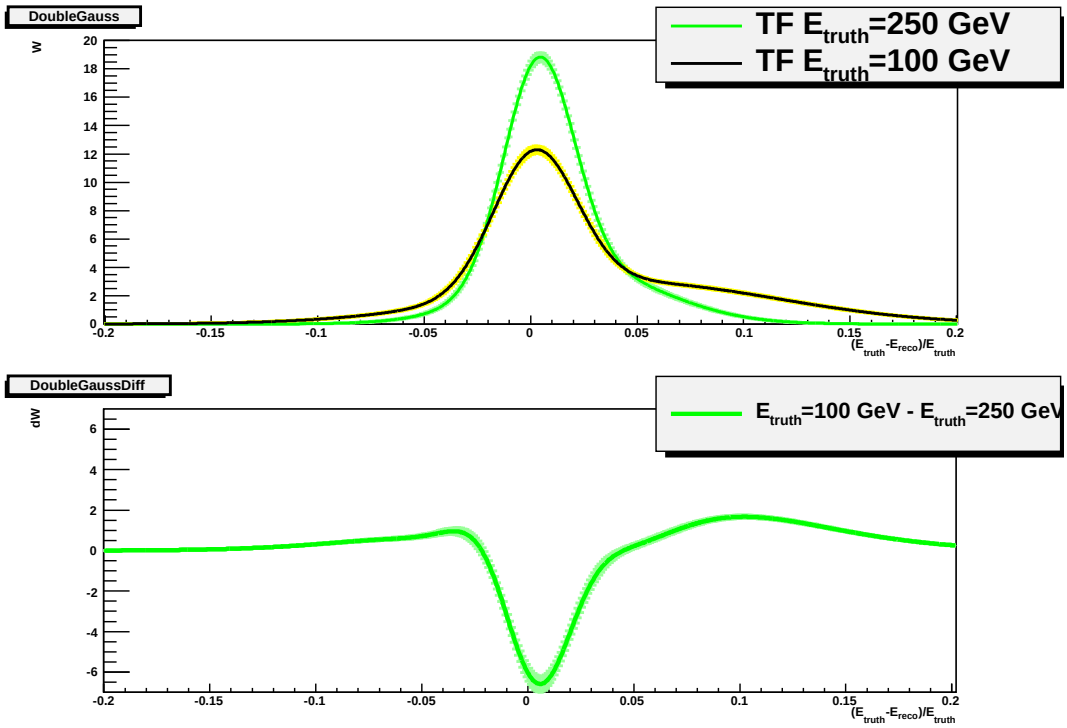

Figure 5.6: Transfer functions for MC10b electrons in the eta region $|\eta| \in [1.52; 2.5]$.

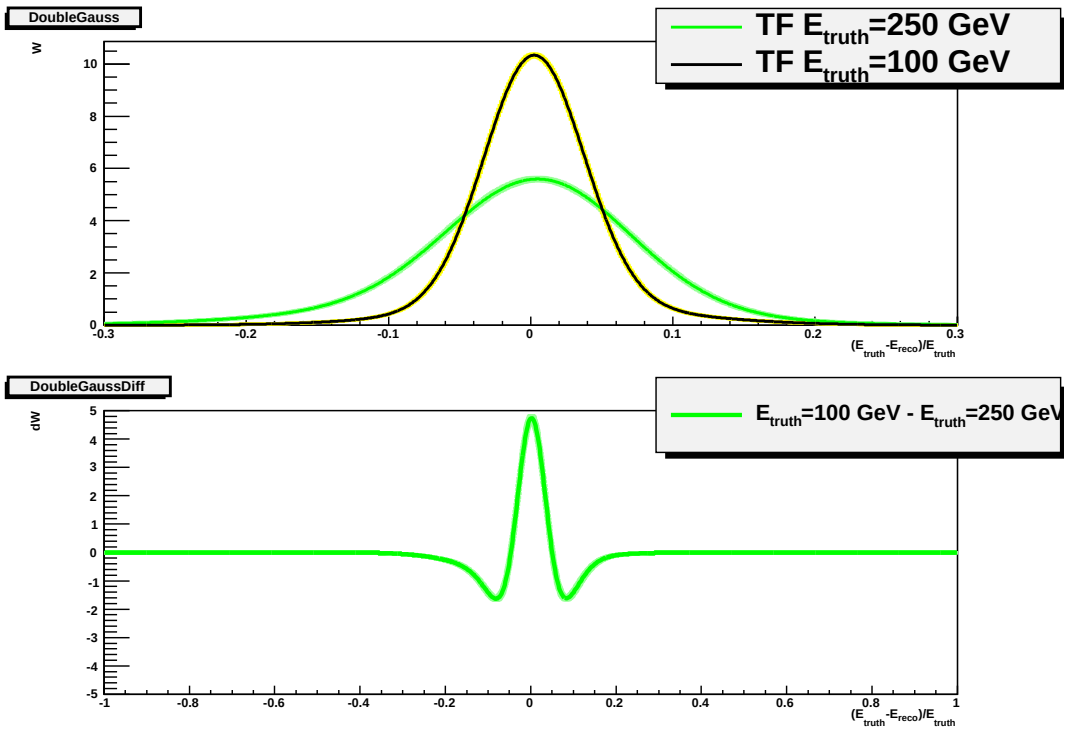

Figure 5.7: Transfer functions for MC10b muons in the eta region $|\eta| \in [0; 1.11]$.

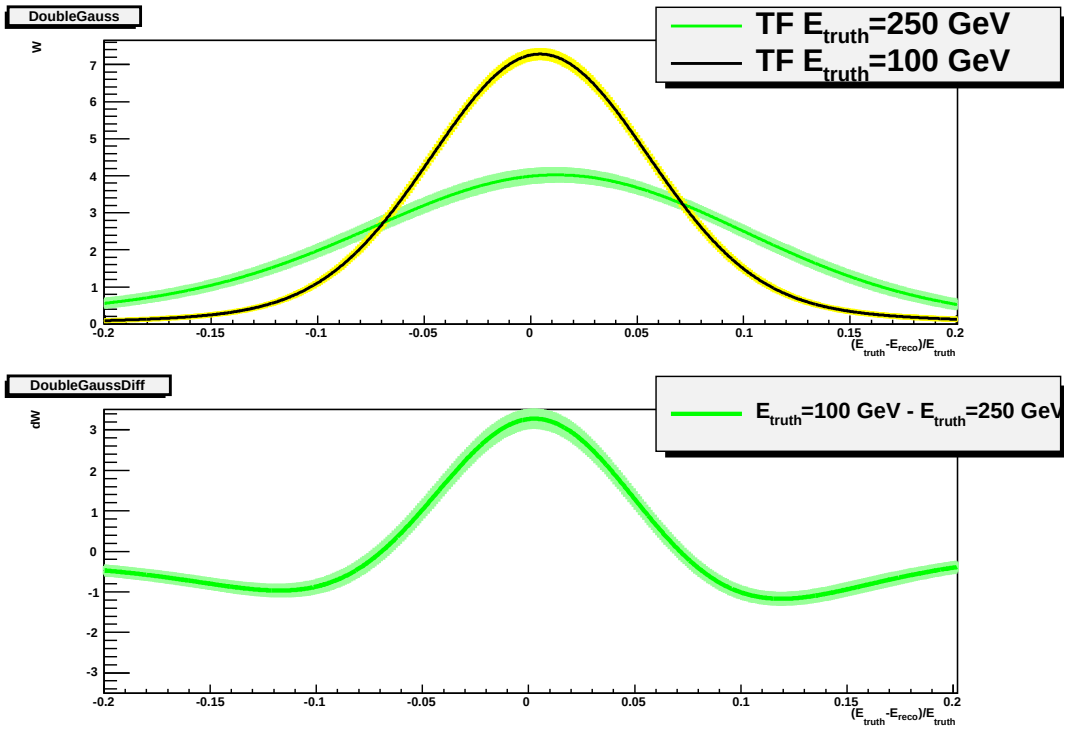

Figure 5.8: Transfer functions for MC10b muons in the eta region $|\eta| \in [1.25; 2.5]$.

proportional to the truth energy while the other partons widths are proportional to $\frac{1}{\sqrt{E_{truth}}}$.

5.1 Fit Range

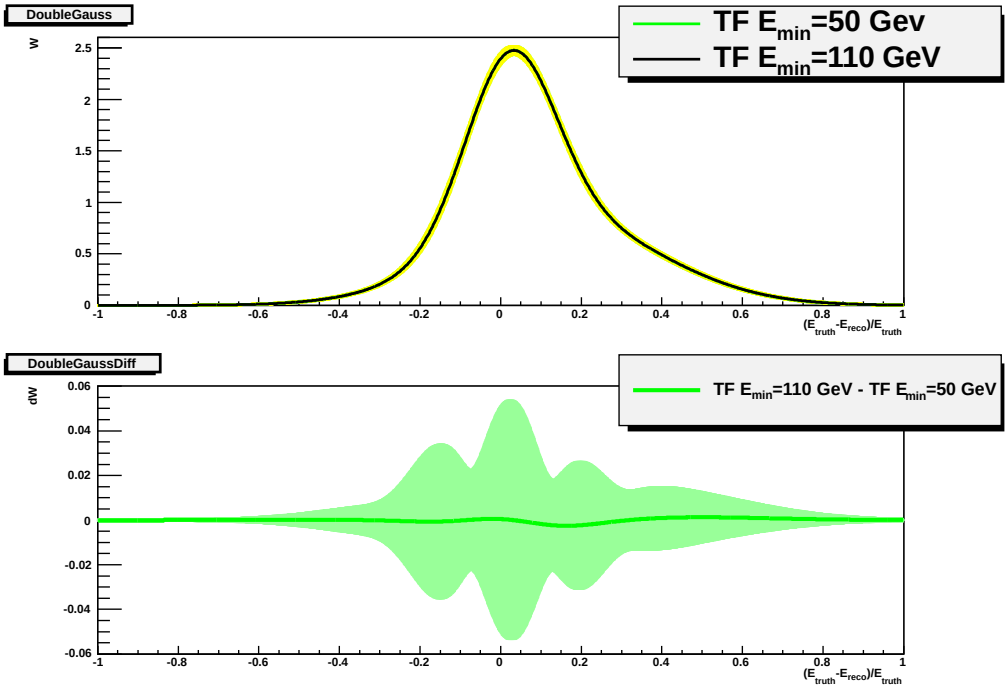

Figure 5.9: Transfer functions for Moriond b-jets in the eta region $|\eta| \in [0; 0.8]$ at 100 GeV. The difference between the transfer functions is so small that one of the functions is covered completely by the other.

The figures 5.9, 5.10, 5.11 and 5.12 show the comparison of transfer functions with different fit ranges. The difference between the transfer functions generated with a lower cut and the ones with a high cut is small. The uncertainty on the differences is large itself, compared to the difference making it within the uncertainties compatible with zero.

The figures 5.12 and 5.13 show this difference for light jets at different energies. Though the difference becomes greater at higher energies, it is still compatible with zero.

Lowering the cut for the fit range is a way to increase statistics, but it also increases the uncertainties of the transfer functions because the points taken into account by lowering the cut tend to differ from the function fitted to the points at higher energy. This can be seen for parameter p_0 for b-jets in figure 5.14. The effect on the transfer function itself is low though because even if a single point of the local fit at low energy is off the fit is still close to what it would be without that point because the majority of points from the local fit are at high energy.

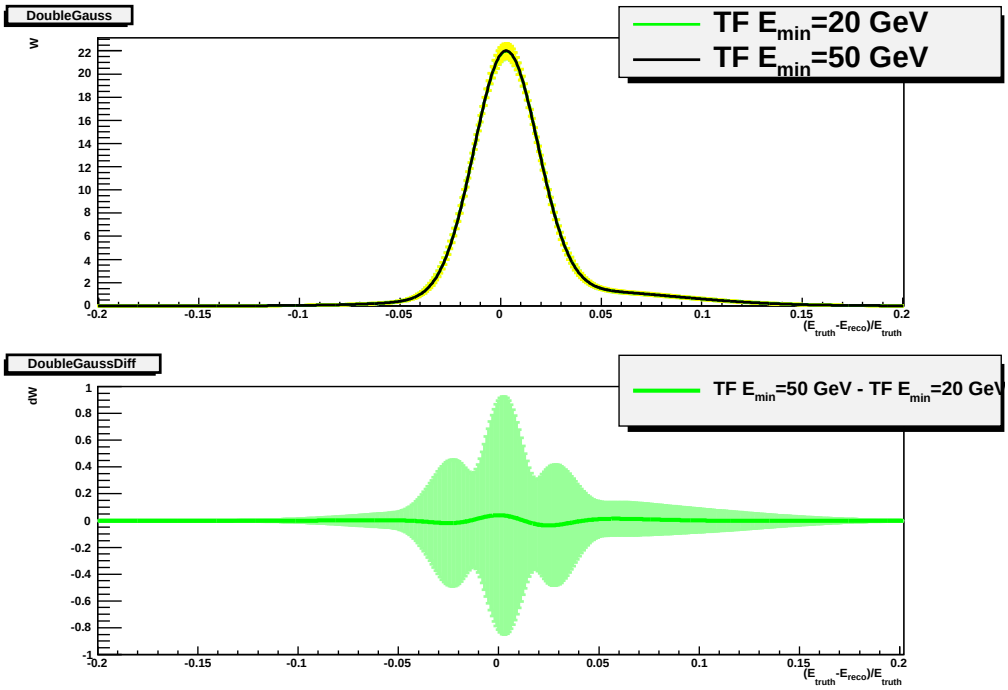

Figure 5.10: Transfer functions for Moriond electrons in the eta region $|\eta| \in [0; 0.8]$ at 100 GeV. The difference between the transfer functions is so small that one of the functions is covered completely by the other.

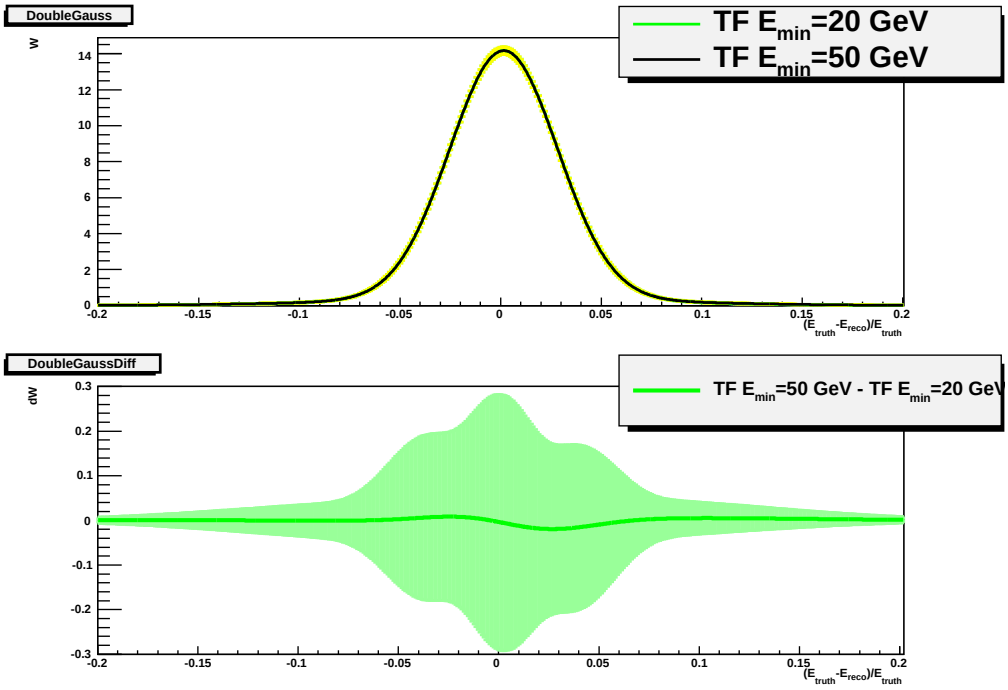

Figure 5.11: Transfer functions for Moriond muons in the eta region $|\eta| \in [0; 1.11]$ at 100 GeV. The difference between the transfer functions is so small that one of the functions is covered completely by the other.

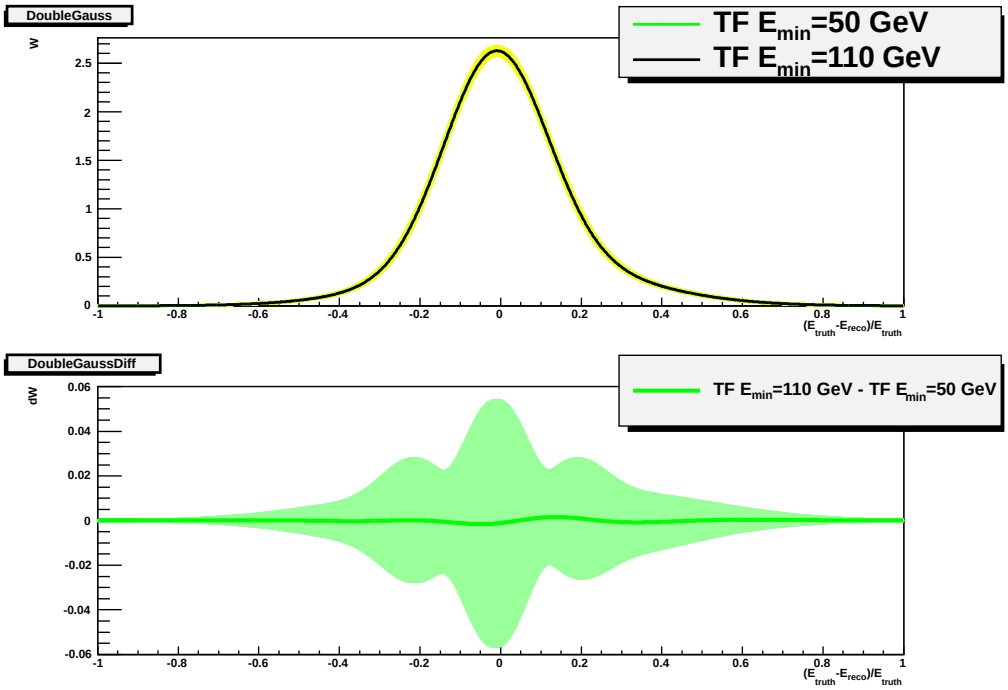

Figure 5.12: Transfer functions for Moriond light jets in the eta region $|\eta| \in [0; 0.8]$ at 100 GeV. The difference between the transfer functions is so small that one of the functions is covered completely by the other.

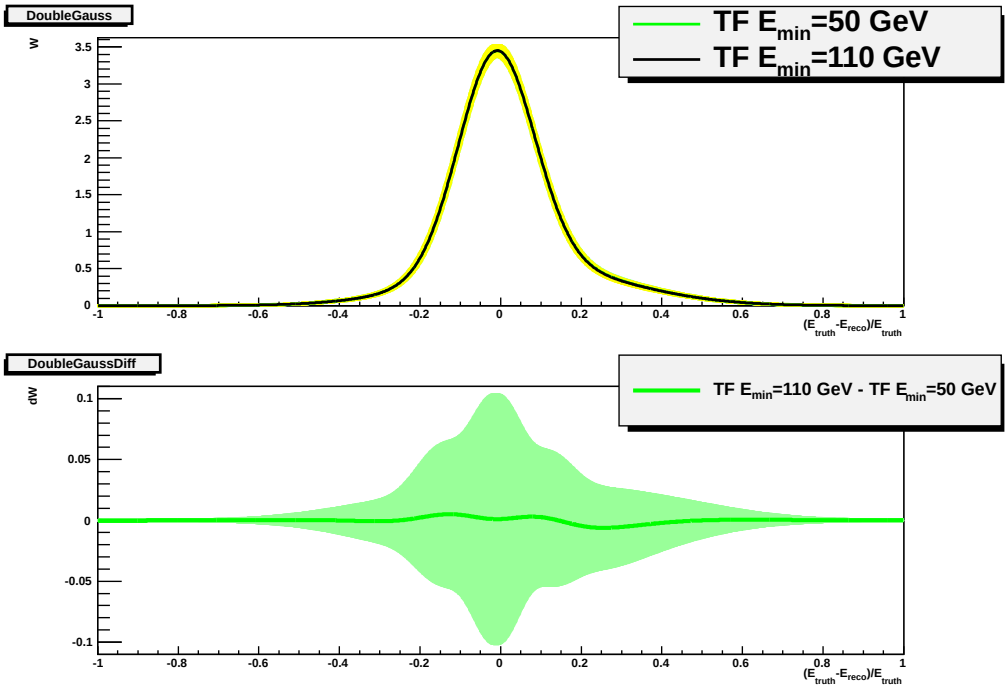

Figure 5.13: Transfer functions for Moriond light jets in the eta region $|\eta| \in [0; 0.8]$ at 250 GeV. The difference between the transfer functions is so small that one of the functions is covered completely by the other.

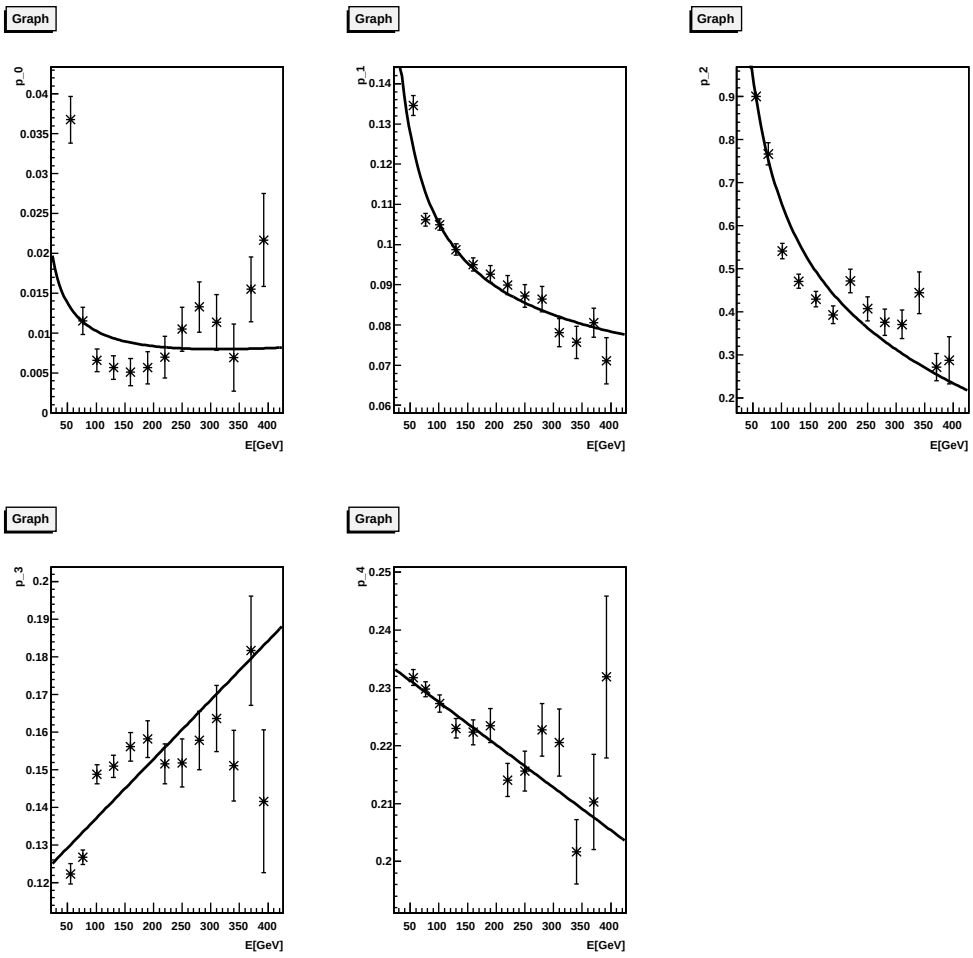

Figure 5.14: Fit to the parameters from the local fit using the lower E_{min} cut.

5.2 Matching Radius

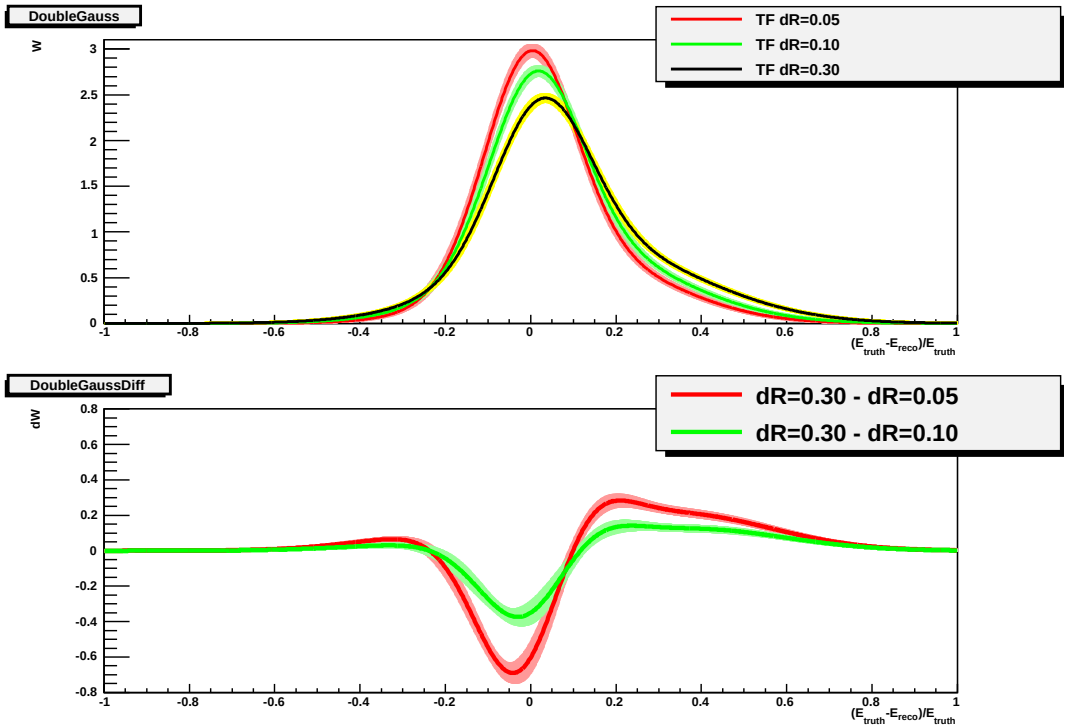

Figure 5.15: Transfer functions for Moriond b-jets in the eta region $|\eta| \in [0; 0.8]$ at 100 GeV.

Shown in the figures 5.15, 5.16, 5.17 and 5.18 are the transfer functions for different matching radii. The difference to the currently used transfer functions with $dR = 0.3$ is relatively small for electrons and muons, but large for jets. This is caused by the calorimeter entries of electrons being much more compact than the ones of jets which deposit energy in the calorimeter with a lower resolution. Higher matching radii shift the transfer functions to higher values of $\frac{E_{truth}-E_{reco}}{E_{truth}}$. This is caused by split-offs from jets which shift the jet axis away from the partons axis and causing energy loss. Little energy is lost for low matching radii as they do not take these events into account because the shifted jet axis is too far away from the partons axis.

Figure 5.19 shows the difference for light jets at high energies. The difference is smaller than the one at lower energies.

Different matching radii lead to different transfer functions and thus it is necessary to use transfer functions with a matching radius of $dR = 0.3$ because most analyses use event selections which allow jets with a large cone und thus a higher probability for larger

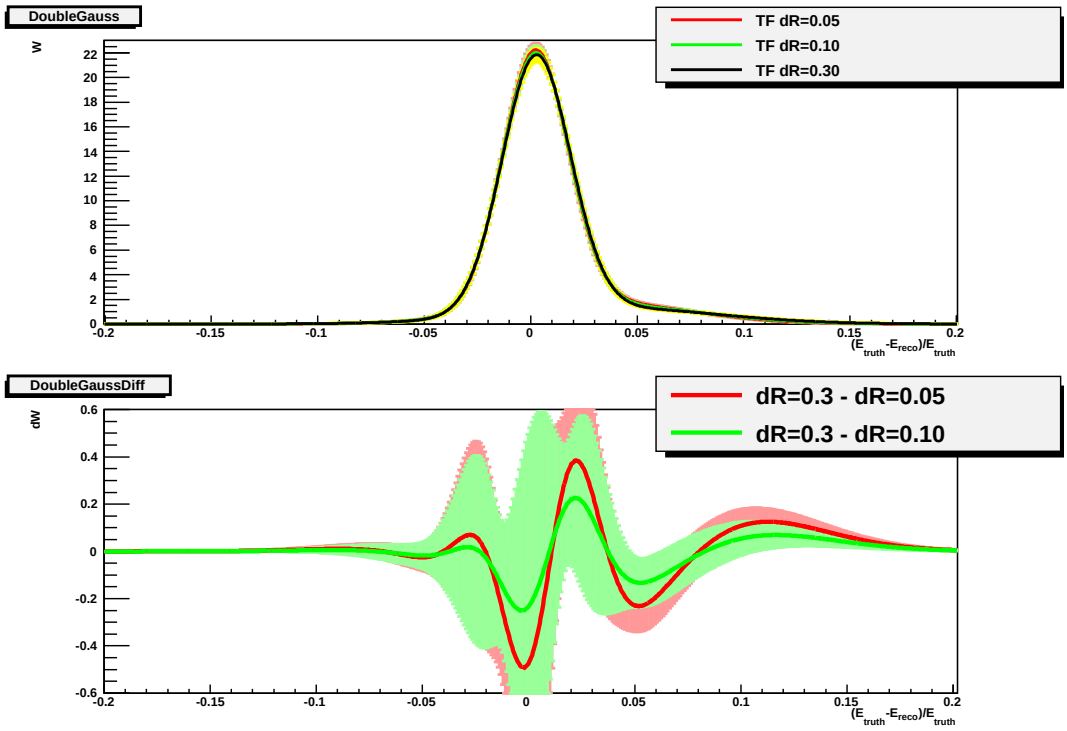

Figure 5.16: Transfer functions for Moriond electrons in the eta region $|\eta| \in [0; 0.8]$ at 100 GeV.

distances to the parton axis to be taken into account. For analyses only allowing tight jets it is advisable to use transfer functions with a lower matching radius.

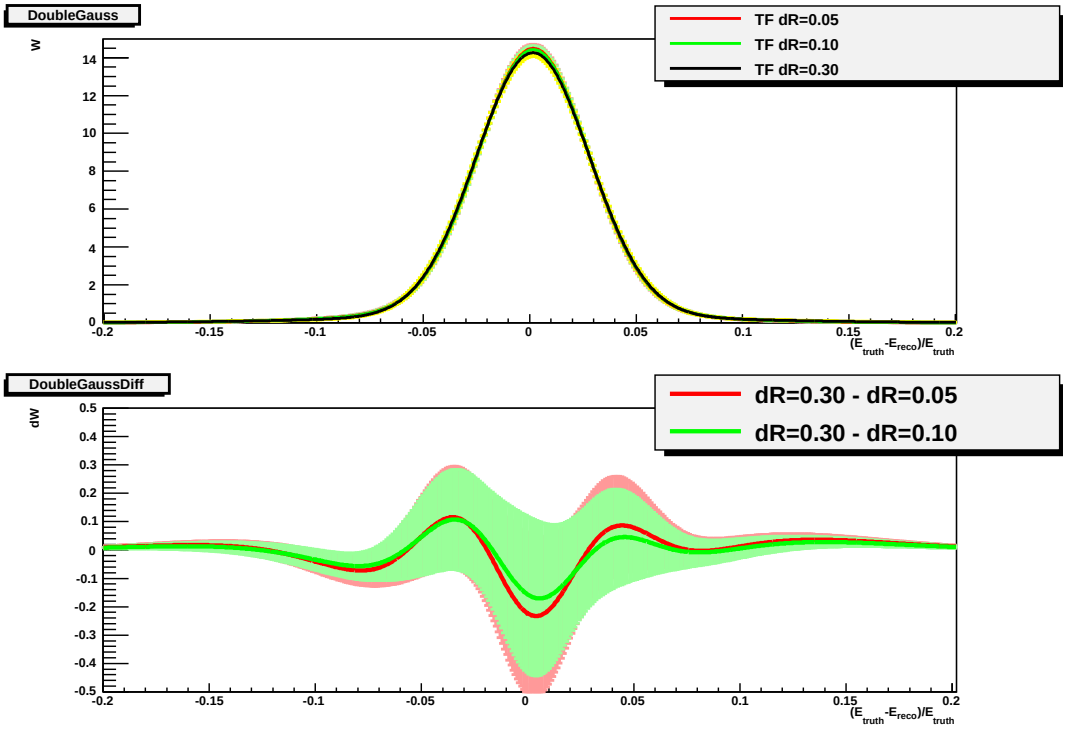

Figure 5.17: Transfer functions for Moriond muons in the eta region $|\eta| \in [0; 1.11]$ at 100 GeV.

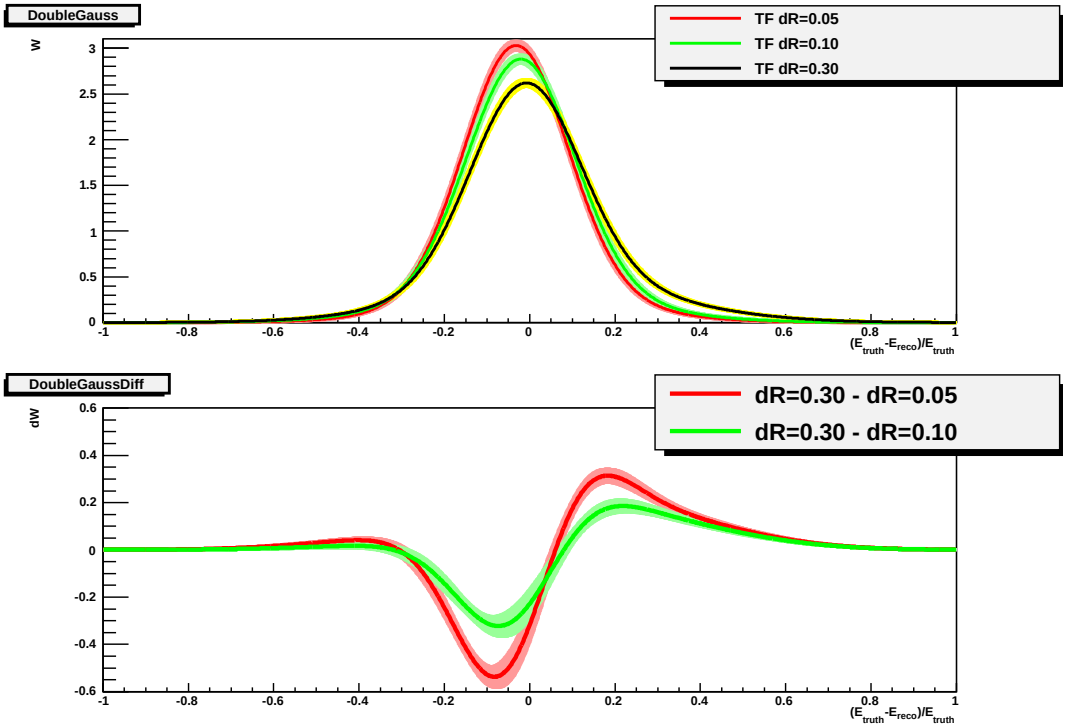

Figure 5.18: Transfer functions for Moriond light jets in the eta region $|\eta| \in [0; 0.8]$ at 100 GeV.

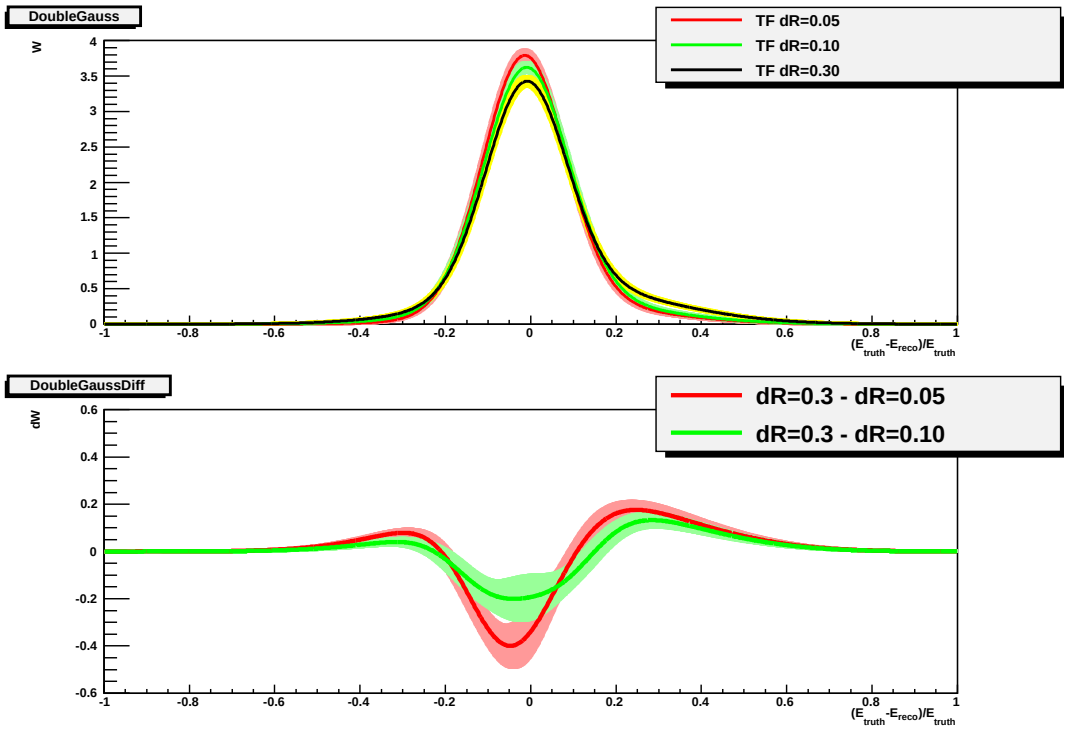

Figure 5.19: Transfer functions for Moriond light jets in the eta region $|\eta| \in [0; 0.8]$ at 250 GeV.

5.2.1 KLFitter results

The transfer functions for the matching radii $dR = 0.30$ and $dR = 0.10$ haven been used in KLFitter to compare the results.

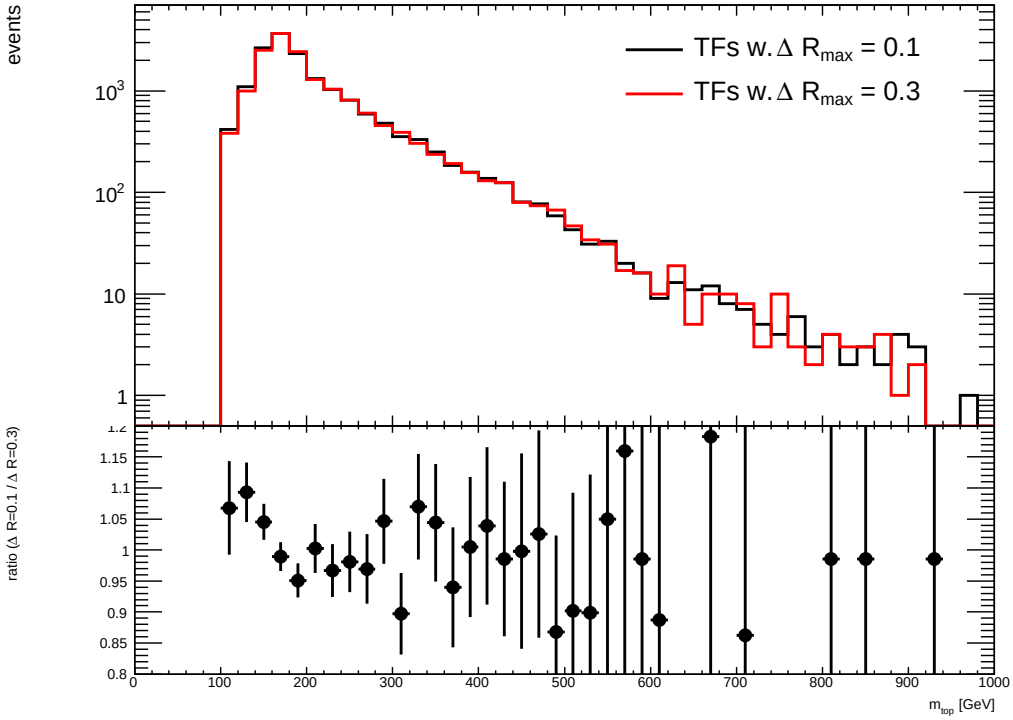

Figure 5.20: Comparision of the hadronic top mass delivered by KLFitter. The upper plot shows the number of events per energy bin. The lower plot shows the ratio of the two histograms.

The transfer functions with $dR = 0.10$ shift the mass distributions slightly to lower energies and the p_T distribution to lower p_T (figures 5.20, 5.21 and 5.22). This results from the transfer functions with $dR = 0.10$ being narrower than the ones with $dR = 0.30$ (figure 5.18), thus limiting the jet resolution. This leads to smaller mass and p_T spectra. But these effects are small.

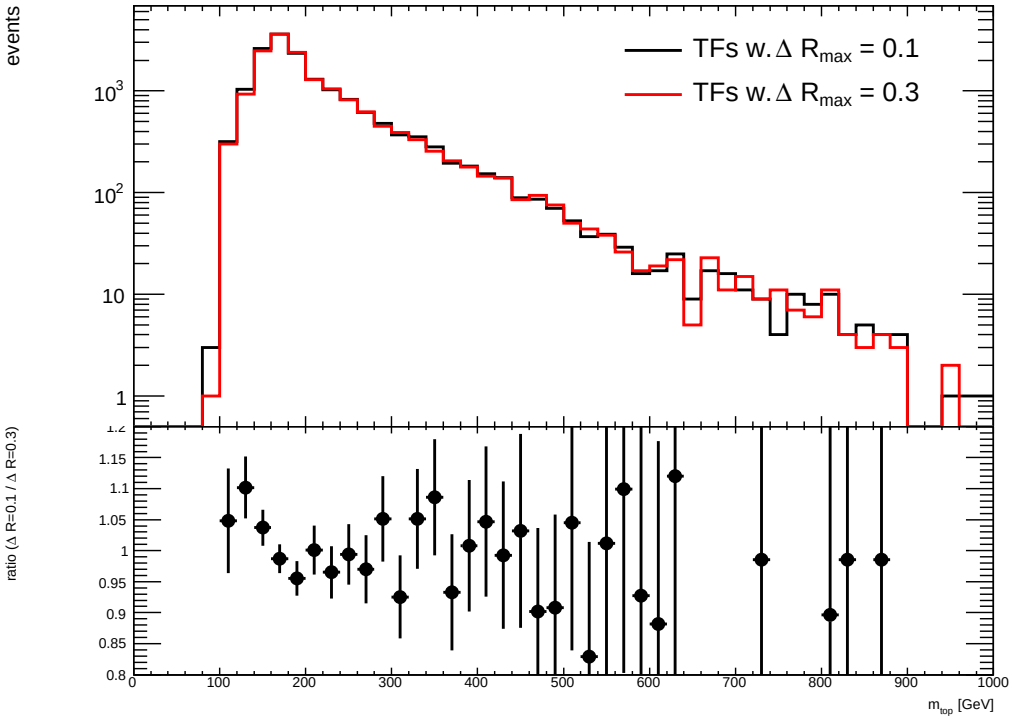

Figure 5.21: Comparision of the leptonic top mass delivered by KLFitter.

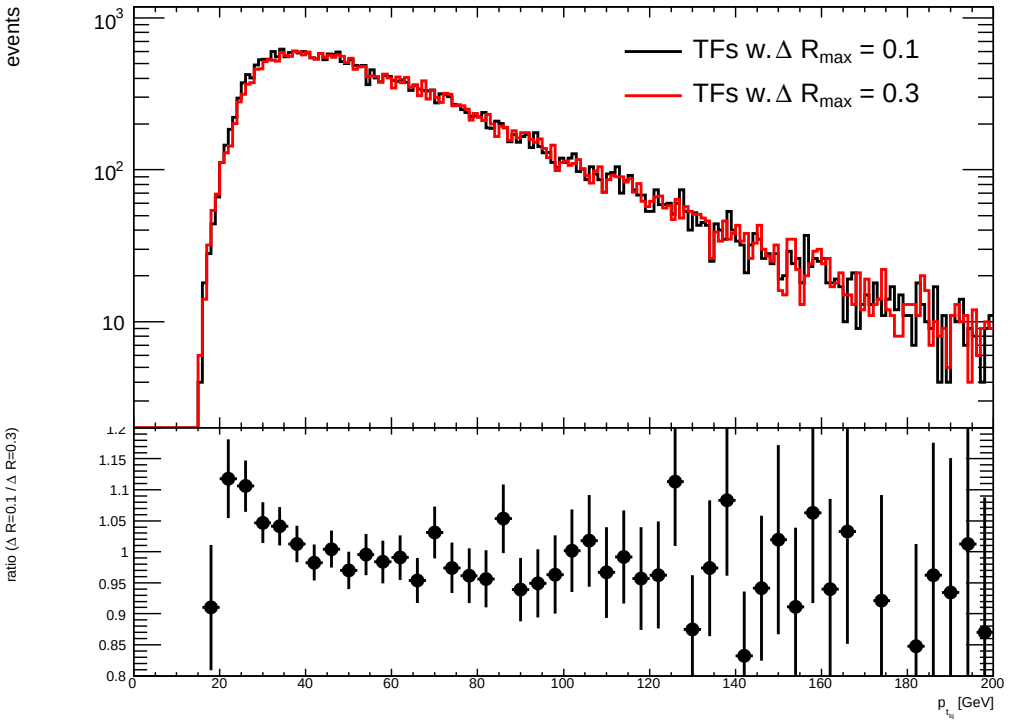

Figure 5.22: Comparision of the p_T of the light jets delivered by KLFitter.

5.3 Top Mass

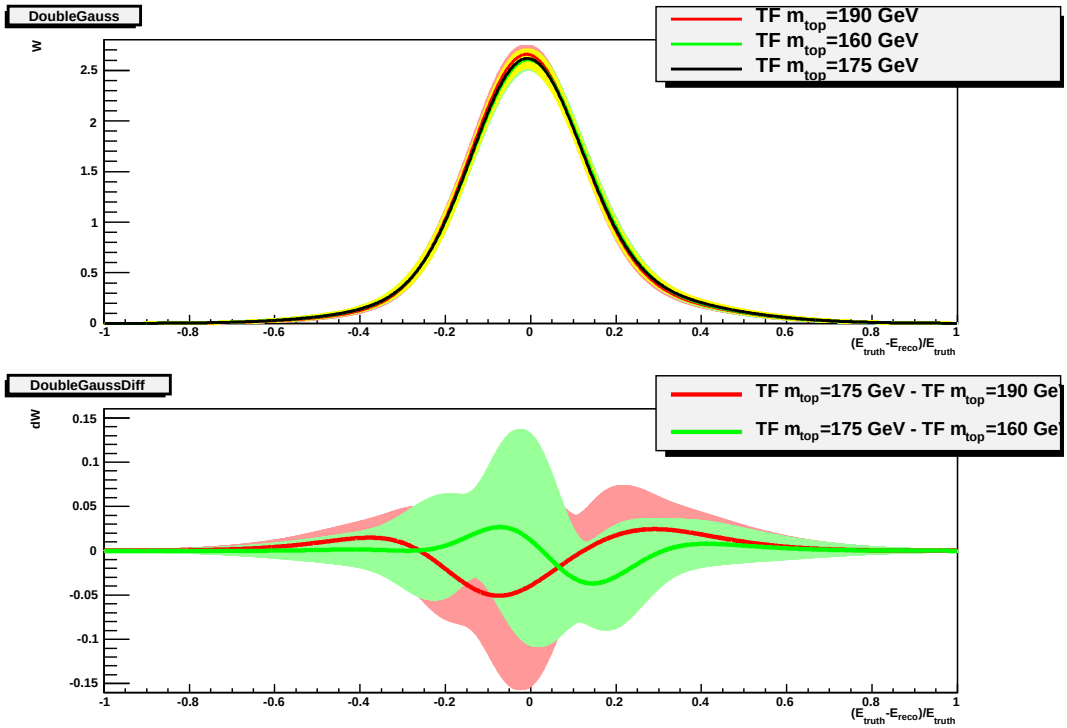

Figure 5.23: Transfer functions for Moriond light jets in the eta region $|\eta| \in [0; 0.8]$ at 100 GeV.

The figures 5.23, 5.24, 5.25 and 5.26 show the transfer functions calculated using MC samples with different top quark masses. For the eta region $|\eta| \in [0; 0.8]$ for jets and electrons and 0.00 to 1.11 for muons the difference between the transfer functions is small and due to their uncertainties compatible with zero.

For higher truth energies the difference grows, but is compatible with zero as shown for light jets in figure 5.27.

For high $|\eta|$ regions the difference between the transfer functions becomes large for electrons. Figure 5.28 shows the transfer functions for electrons in the $|\eta|$ region $|\eta| \in [1.52; 2.5]$. The transfer functions created using the MC samples with the masses 160 GeV and 190 GeV differ greatly from the transfer function calculated using MC samples with a mass of 175 GeV. The uncertaintie of the differences are large enough to make it compatible with zero though. Something similar can be observed for muons though the effect is not as strong (figure 5.29). This effect is not observed for jets (figure 5.30 and 5.31). Low statistics for muons and electrons in these $|\eta|$ regions result in a bad fit which is the cause of this effect.

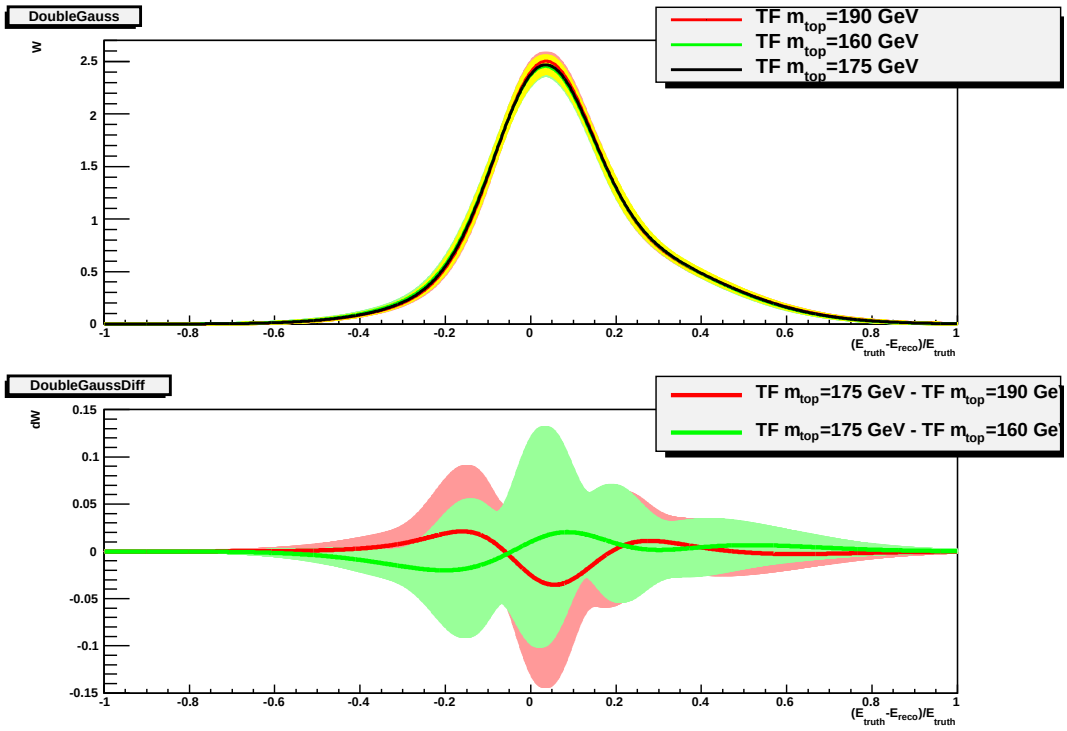

Figure 5.24: Transfer functions for Moriond b-jets in the eta region $|\eta| \in [0; 0.8]$ at 100 GeV.

The mass of the top quark has an influence on the energy distribution of the partons and thus influences the kinematics of an event. The effects which result in the energy of the particles to be reconstructed at a different value than their truth energy like pileup do not change though and so do the transfer functions. Thus MC samples with different top quark masses lead to similar transfer functions which are compatible with each other within their uncertainties. In future analyses these MC samples can be combined to increase statistics. In oder to determine if there is a systematical top quark mass dependance of the transfer functions it is necessary to further decrease the statistical uncertainties by increasing statistics.

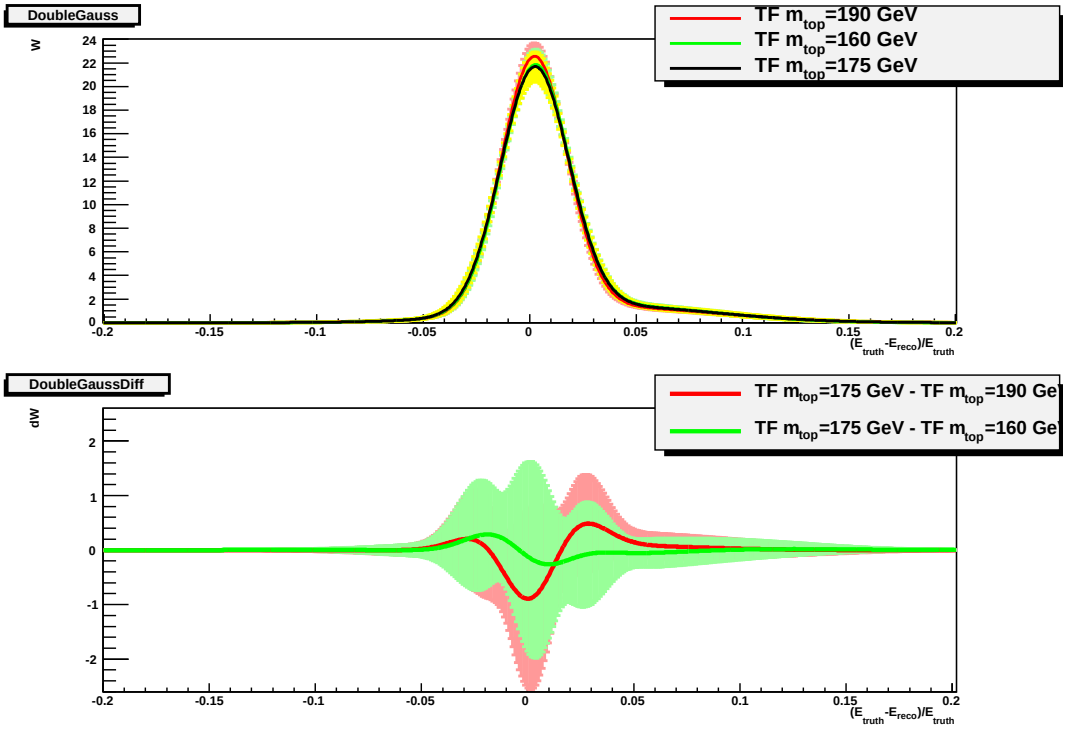

Figure 5.25: Transfer functions for Moriond electrons in the eta region $|\eta| \in [0; 0.8]$ at 100 GeV.

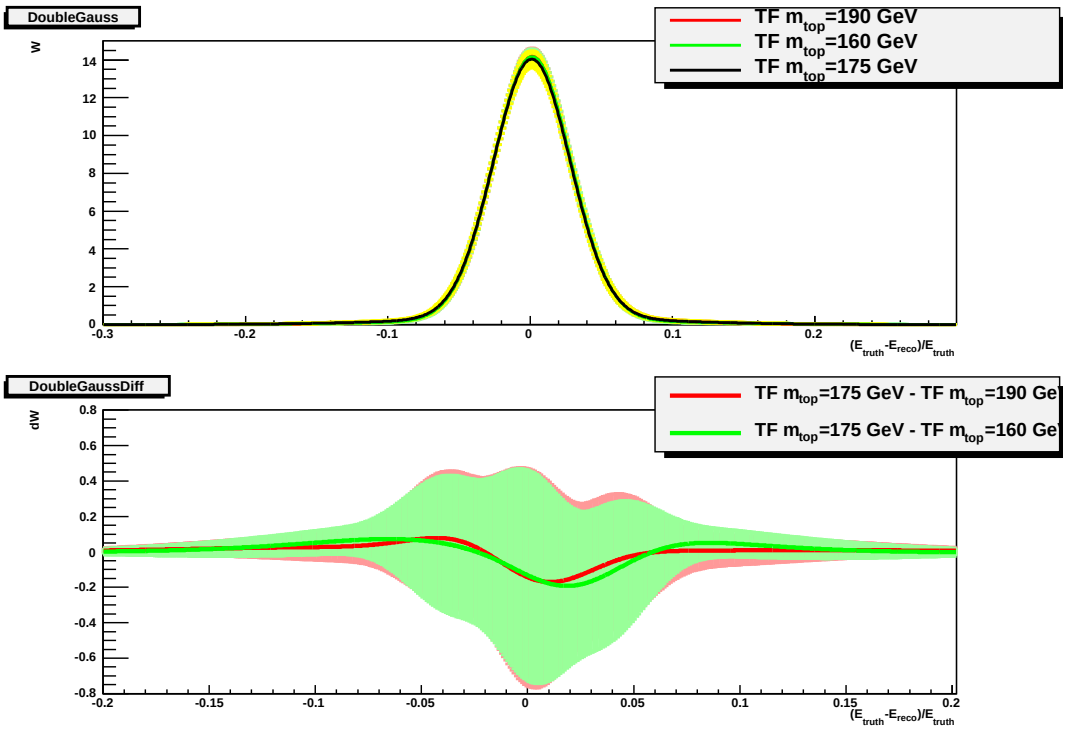

Figure 5.26: Transfer functions for Moriond muons in the eta region $|\eta| \in [0; 1.11]$ at 100 GeV.

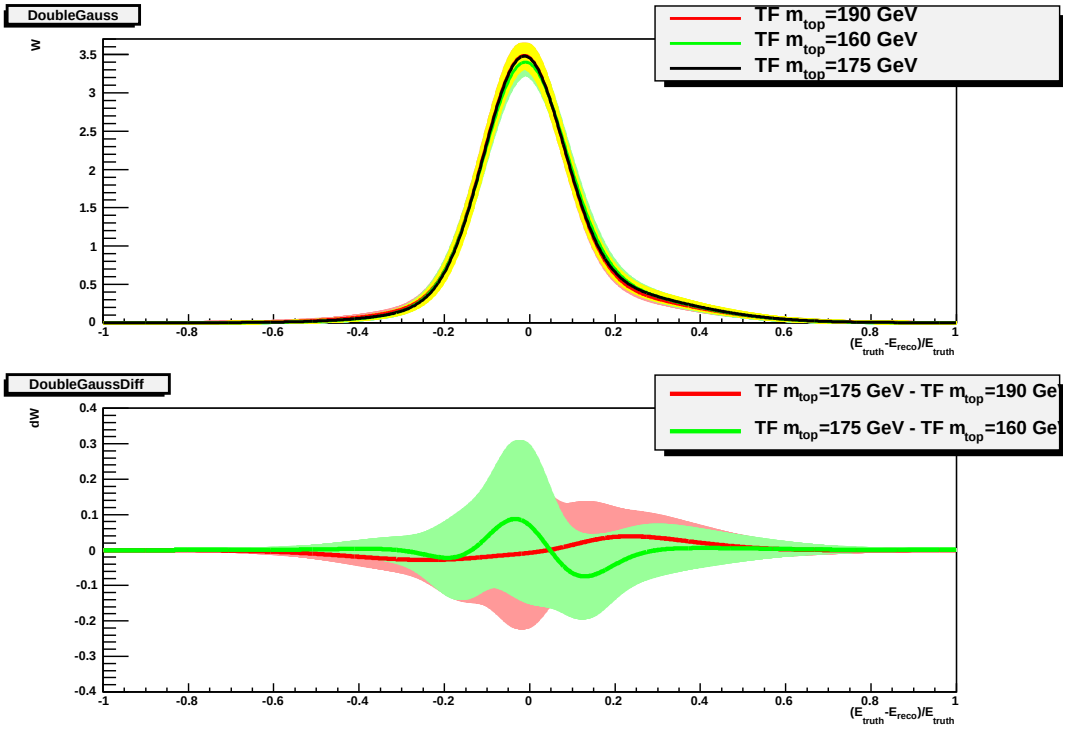

Figure 5.27: Transfer functions for Moriond light jets in the eta region $|\eta| \in [0; 0.8]$ at 250 GeV.

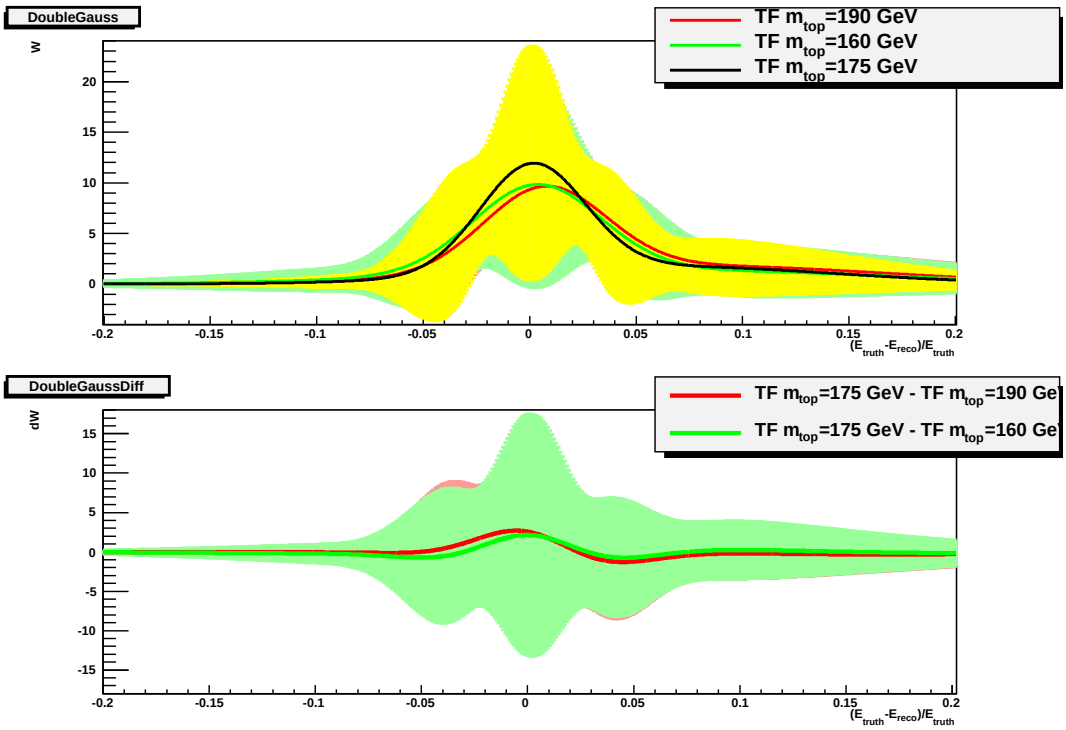

Figure 5.28: Transfer functions for Moriond electrons in the eta region $|\eta| \in [1.52; 2.5]$ at 100 GeV.

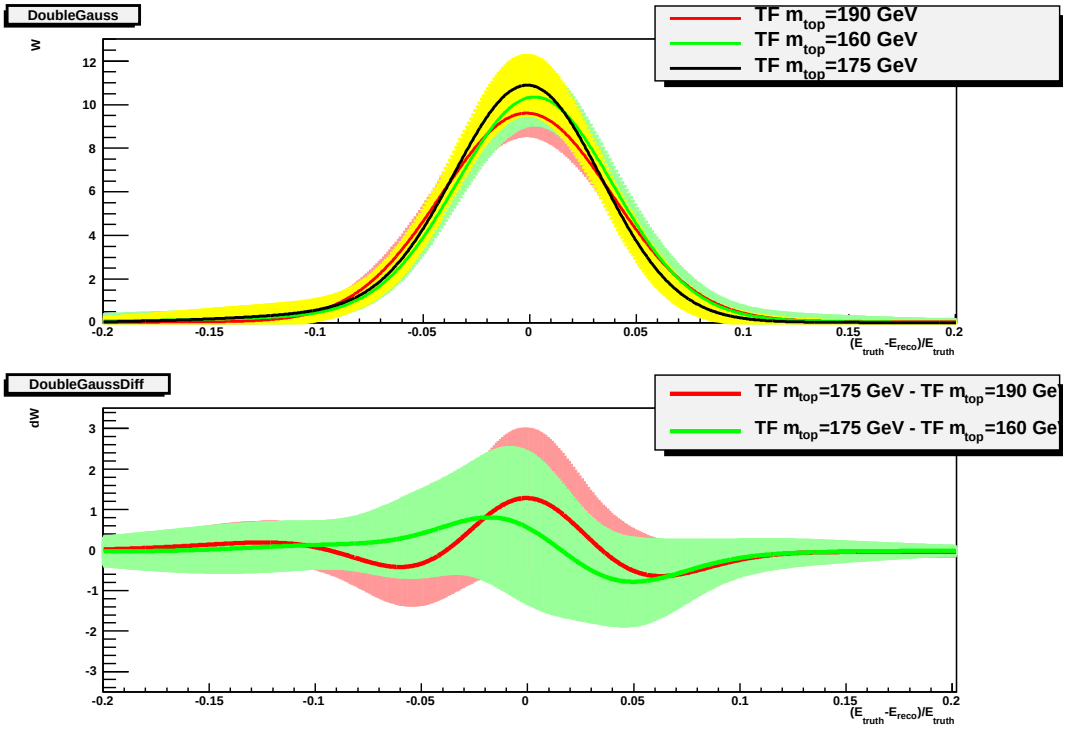

Figure 5.29: Transfer functions for Moriond muons in the eta region $|\eta| \in [1.25; 2.5]$ at 100 GeV.

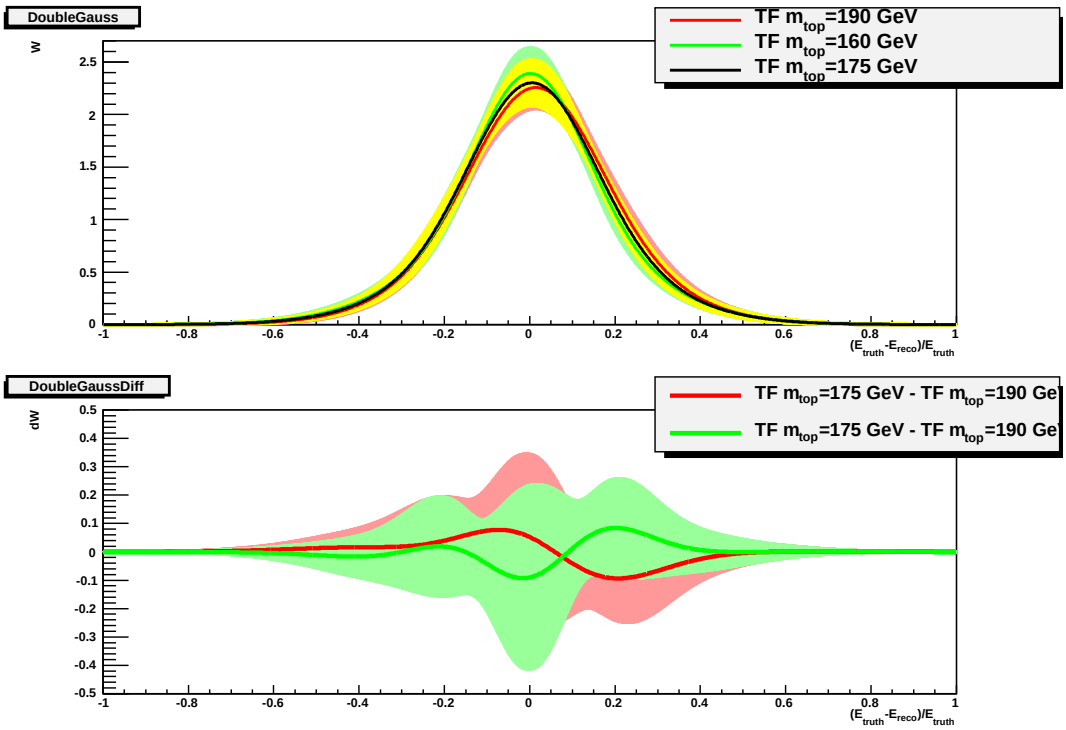

Figure 5.30: Transfer functions for Moriond light jets in the eta region $|\eta| \in [1.52; 2.5]$ at 100 GeV.

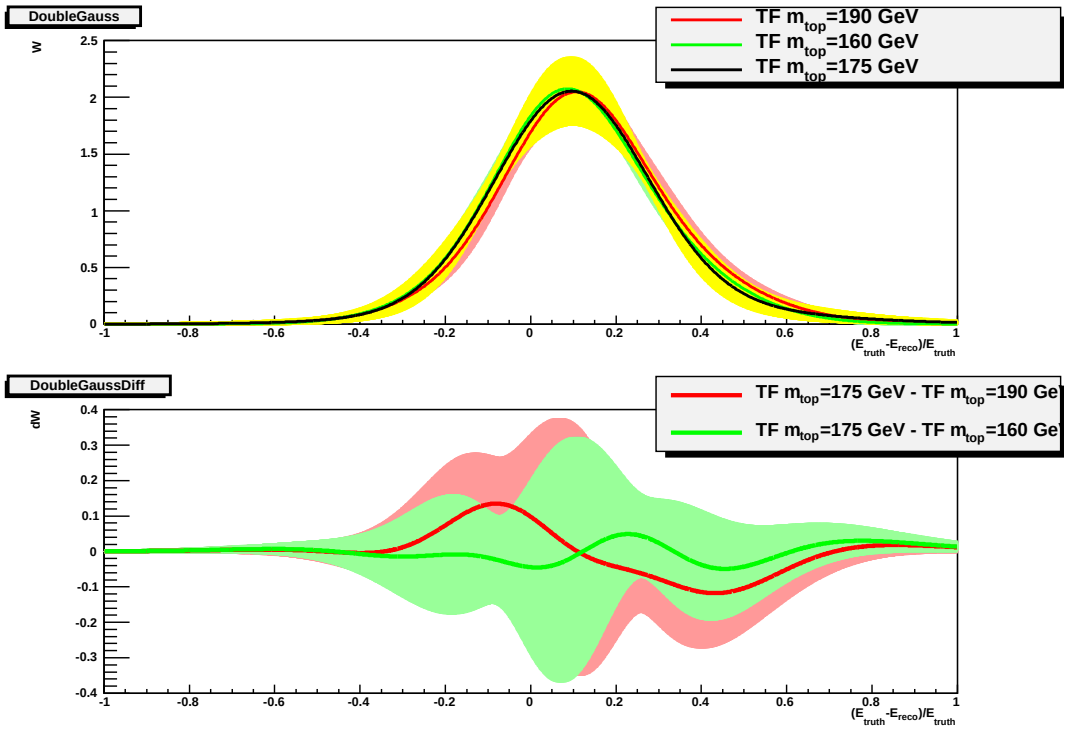

Figure 5.31: Transfer functions for Moriond b-jets in the eta region $|\eta| \in [1.52; 2.5]$ at 100 GeV.

5.4 Parameter Correlations

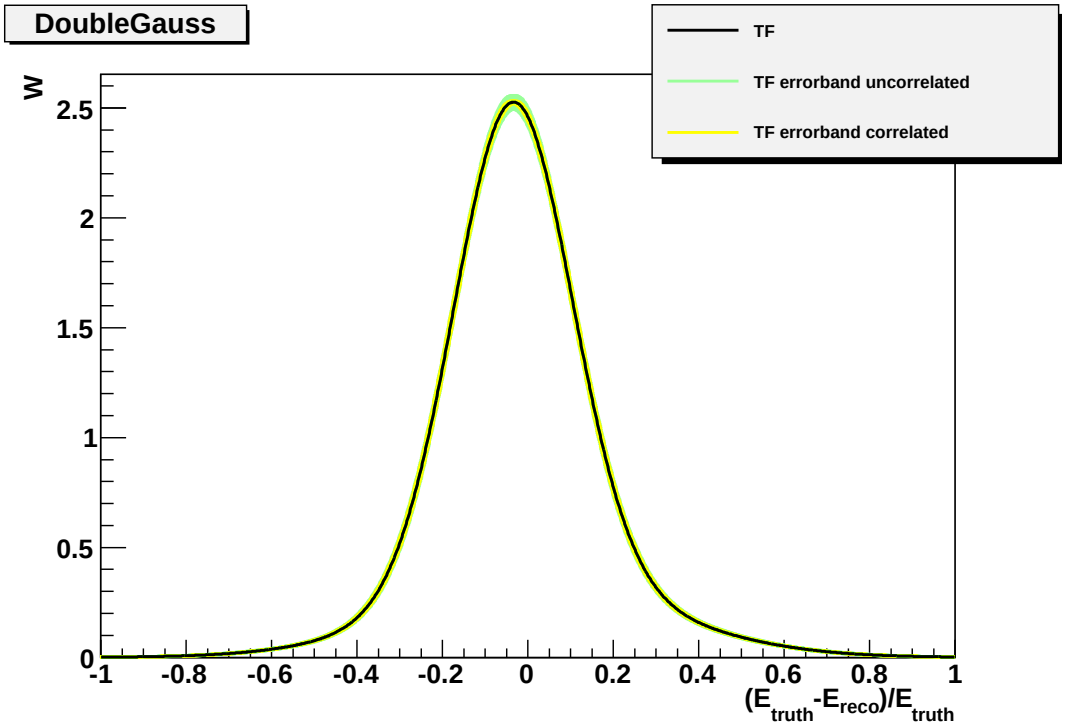

Figure 5.32: Transfer functions for MC10b light jets in the $|\eta|$ region $|\eta| \in [0; 0.8]$ at 100 GeV.

The figures 5.32 and 5.33 show for lights jets the transfer function assuming uncorrelated parameters and the transfer function taking the parameter correlations into account. The transfer functions' uncertainty decreases when the correlations are taken into account.

This decrease is even more noticeable for $|\eta|$ regions with lower statistics e.g. in the $|\eta|$ region $|\eta| \in [1.52; 2.5]$ as shown in the figures 5.34 and 5.35.

The correlations of the parameters of the double Gauss function have a non negligible effect on the uncertainties of the transfer function. Thus when using the transfer functions' uncertainties it is necessary to take these correlations into account.

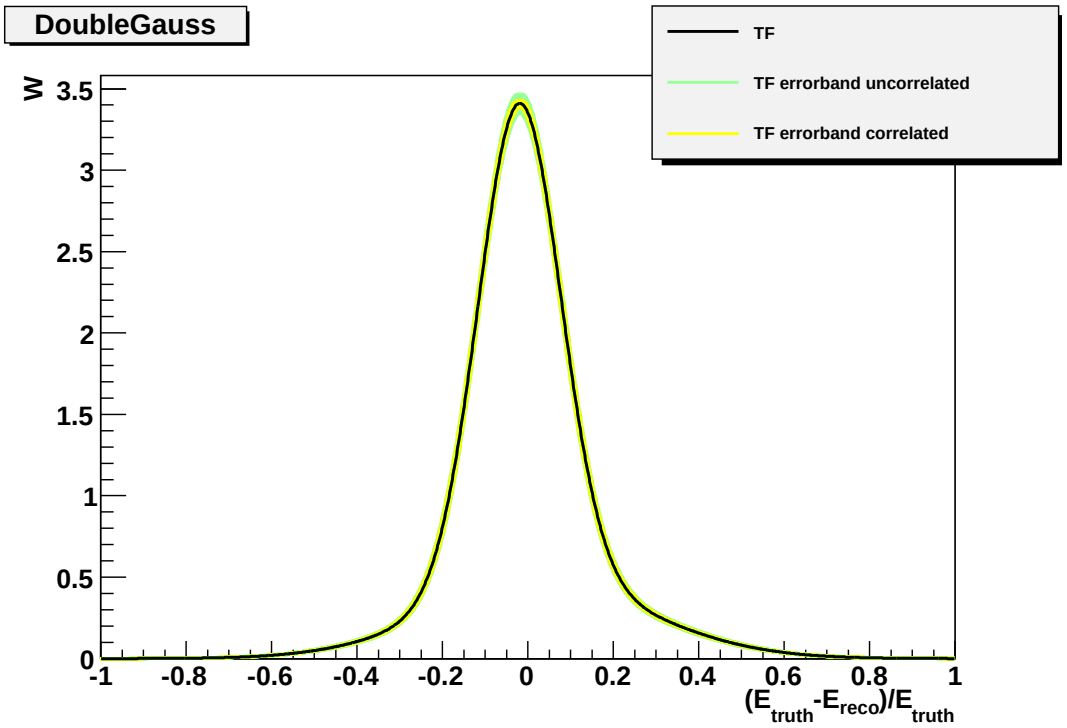

Figure 5.33: Transfer functions for MC10b light jets in the $|\eta|$ region $|\eta| \in [0; 0.8]$ at 250 GeV.

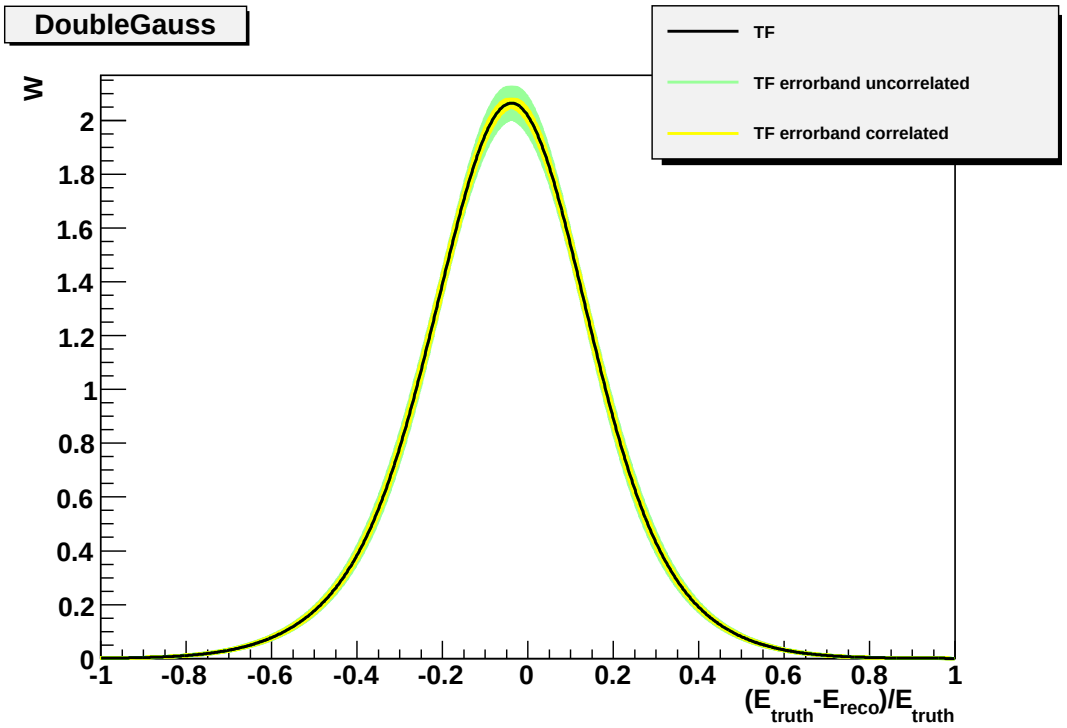

Figure 5.34: Transfer functions for MC10b light jets in the $|\eta|$ region $|\eta| \in [1.52; 2.5]$ at 100 GeV.

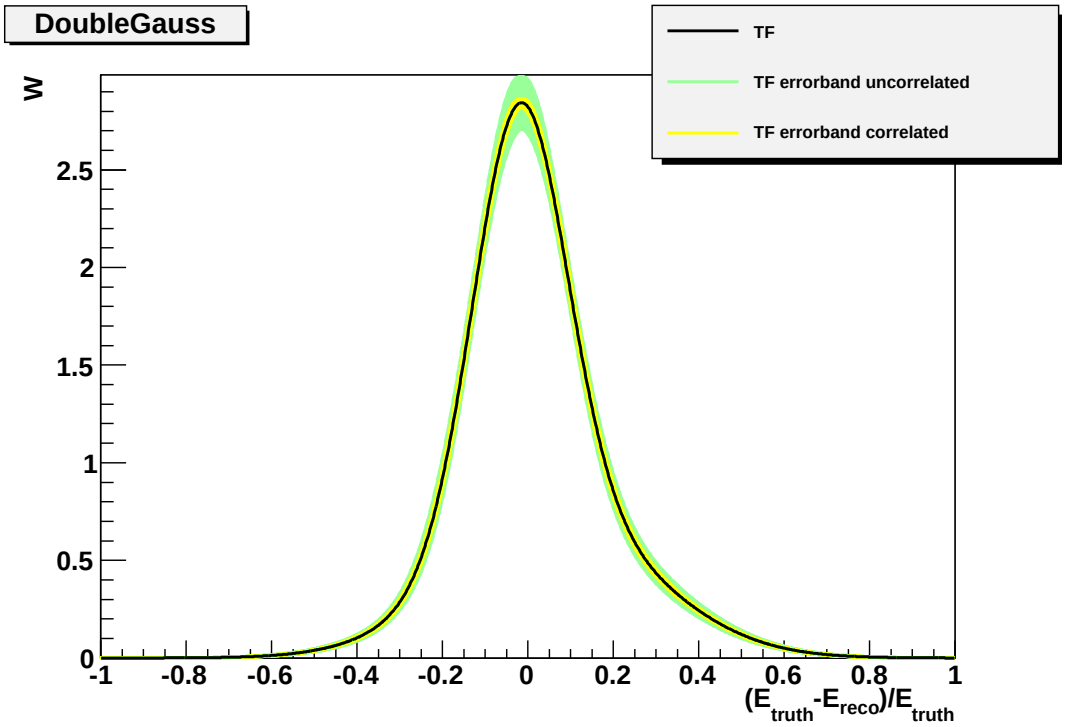

Figure 5.35: Transfer functions for MC10b light jets in the $|\eta|$ region $|\eta| \in [1.52; 2.5]$ at 250 GeV.

5.5 Jet Multiplicity

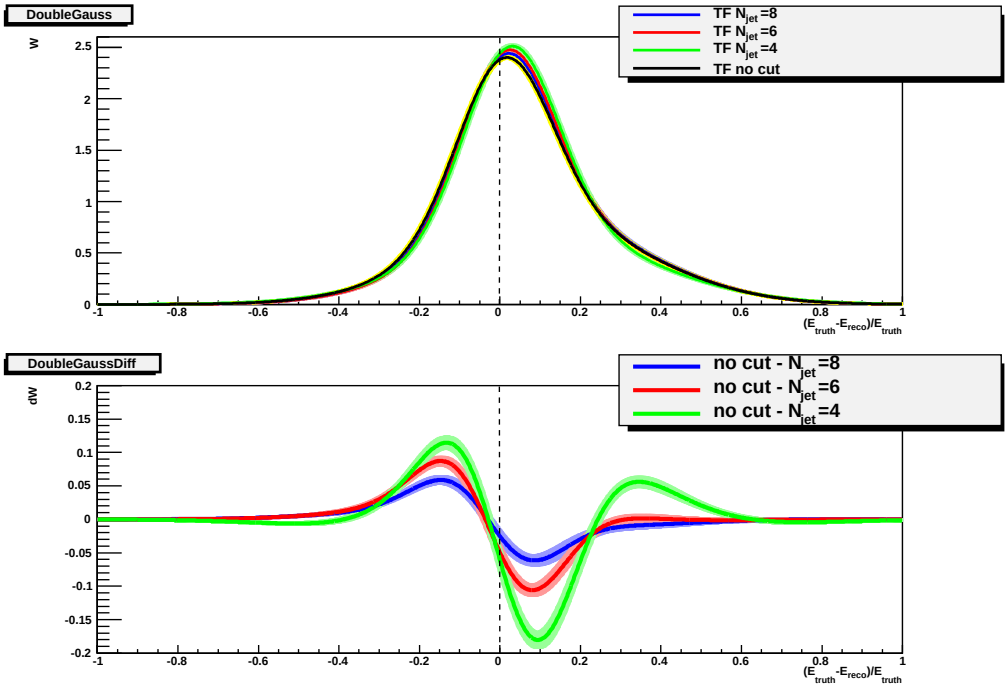

Figure 5.36: Transfer functions for MC10b b-jets in the $|\eta|$ region $|\eta| \in [0; 0.8]$ at 100 GeV.

The figures 5.36, 5.37 and 5.38 show the transfer functions for the jet multiplicity cuts N_{jet} four, six and eight compared to the transfer function without this cut. The lower the cut is the more is the transfer function shifted to higher values of $\frac{E_{truth}-E_{reco}}{E_{truth}}$. The influence on the electron transfer functions is small. The is caused by small jets from the underlying event and pileup being merged with the jets from the $t\bar{t}$ decay during reconstruction. If less jets are allowed less merging occures and so the reconstruced energy is lower.

The effect becomes smaller for higher truth energies. Shown for light jets in figure 5.39. The reason for this is that the energy of the jet created by the underlying event and pileup is small und thus their effect is smaller when the jet they are merged with has high energy.

The maximum jet multiplicity has a non negligible effect on the transfer functions for jets. Thus the transfer functions used in an analysis should use the same jet multiplicity cut as the analysis.

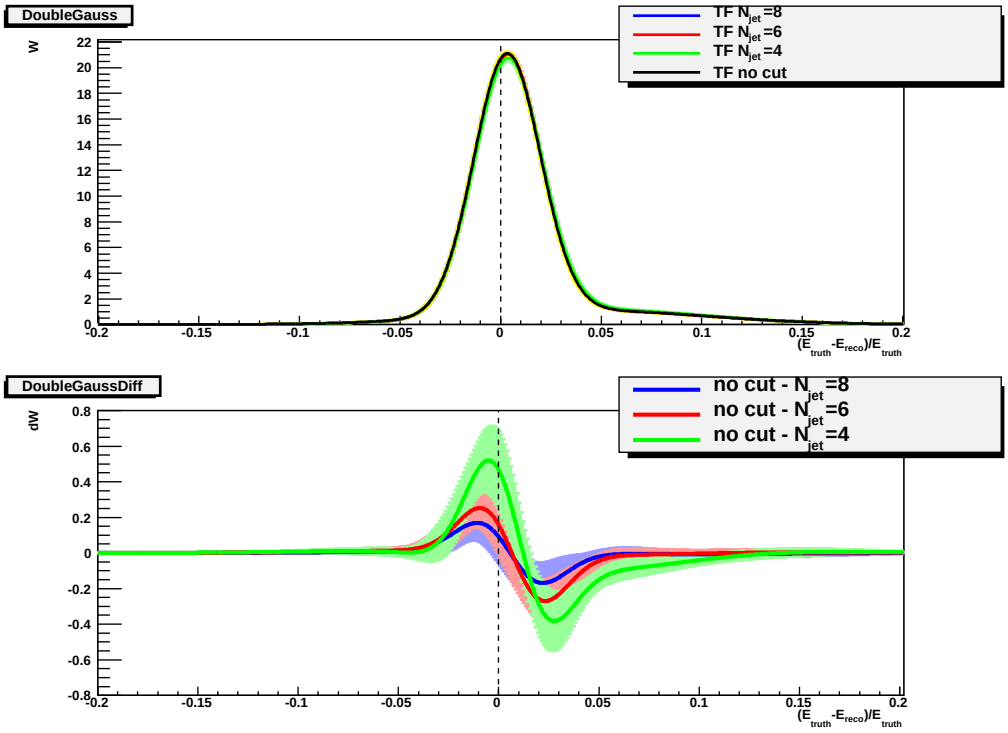

Figure 5.37: Transfer functions for MC10b electrons in the $|\eta|$ region $|\eta| \in [0; 0.8]$ at 100 GeV.

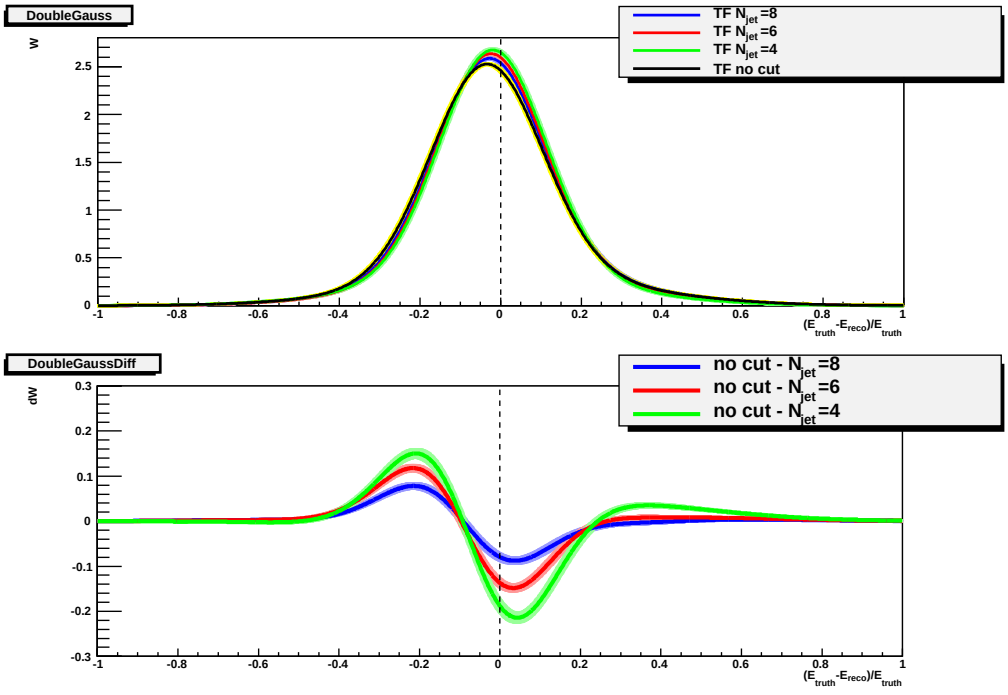

Figure 5.38: Transfer functions for MC10b light jets in the $|\eta|$ region $|\eta| \in [0; 0.8]$ at 100 GeV.

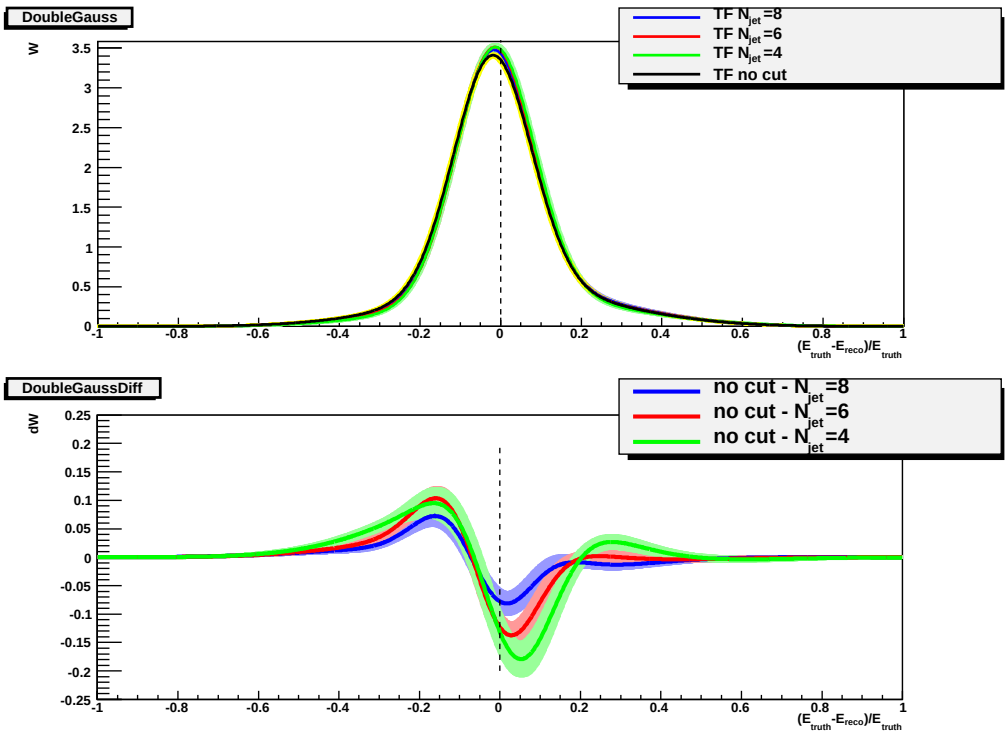

Figure 5.39: Transfer functions for MC10b light jets in the $|\eta|$ region $|\eta| \in [0; 0.8]$ at 250 GeV.

5.6 Event Topology

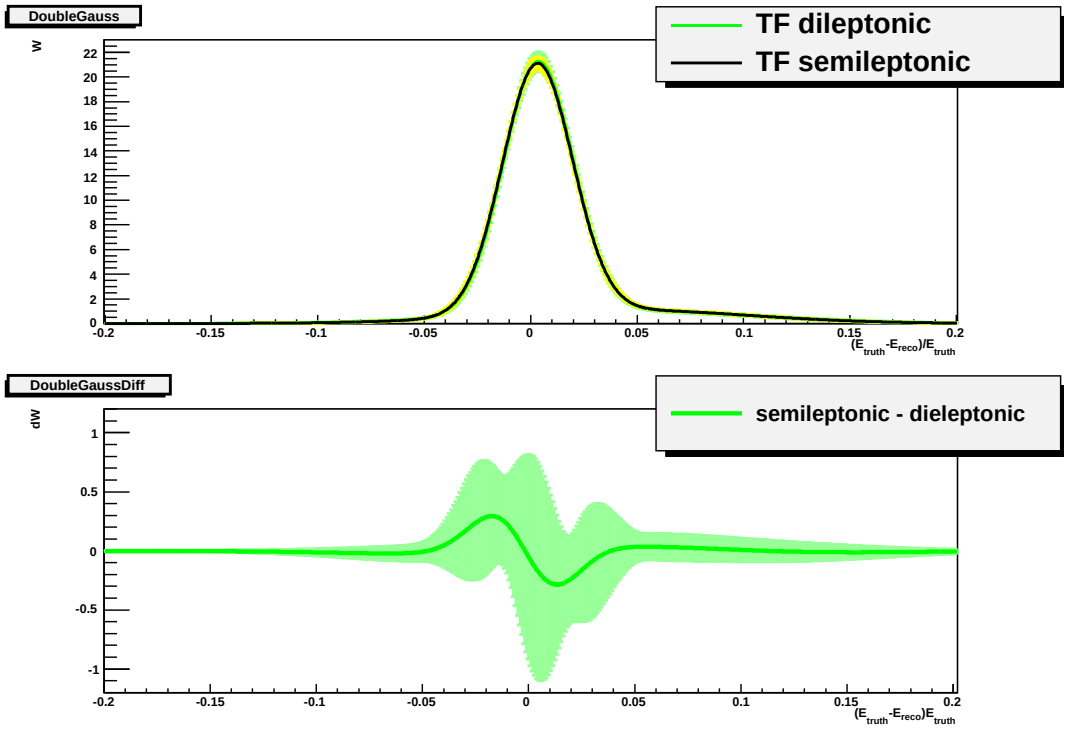

Figure 5.40: Transfer functions for MC10b electrons in the $|\eta|$ region $|\eta| \in [0; 0.8]$ at 100 GeV.

Figure 5.40 shows the comparison of the transfer function calculated from only semileptonic decays to the transfer function calculated from only dileptonic decays. The difference between the transfer functions is small and within their uncertainties compatible with zero. Thus analyses in the semileptonic decay channel can use the same electron transfer functions as analyses in the dileptonic channel and when calculating transfer functions for electrons the MC events from both channels can be merged in order to reach higher statistics. This is not the case for muons as shown in figure 5.41, but this may be a result from a bad fit because for the dileptonic channel one of the limits for the mean value of the second Gauss was set to a wrong value which can have strong impact on the transfer function shown in figure 5.42.

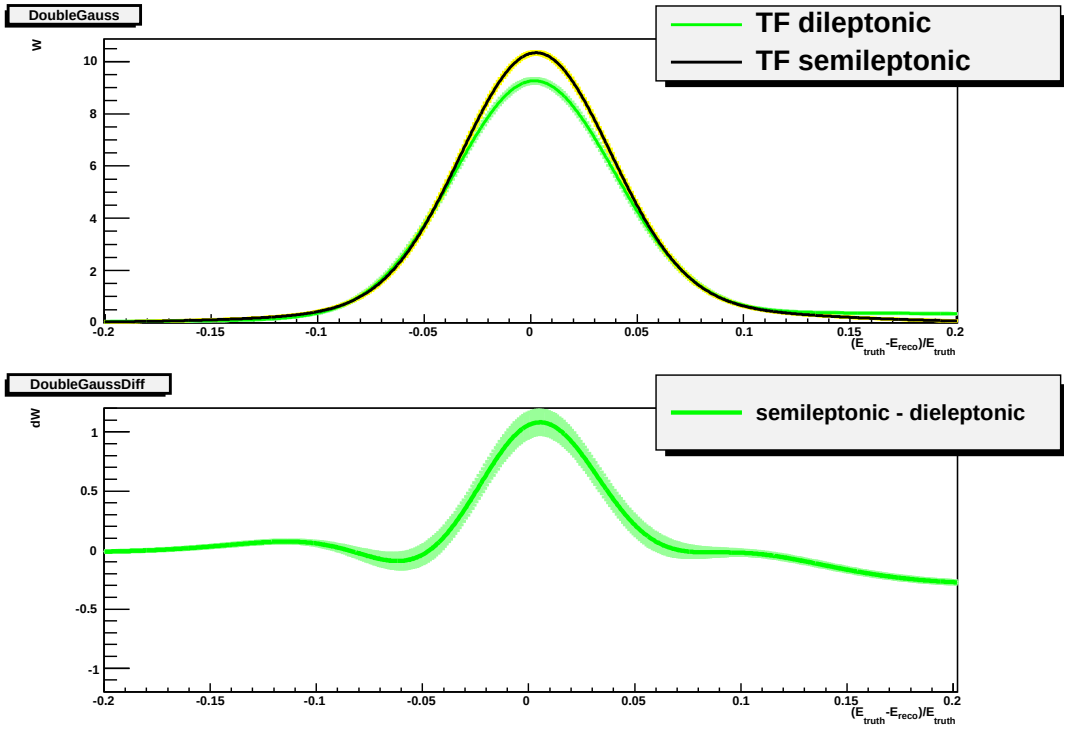

Figure 5.41: Transfer functions for MC10b muons in the $|\eta|$ region $|\eta| \in [0; 1.11]$ at 100 GeV.

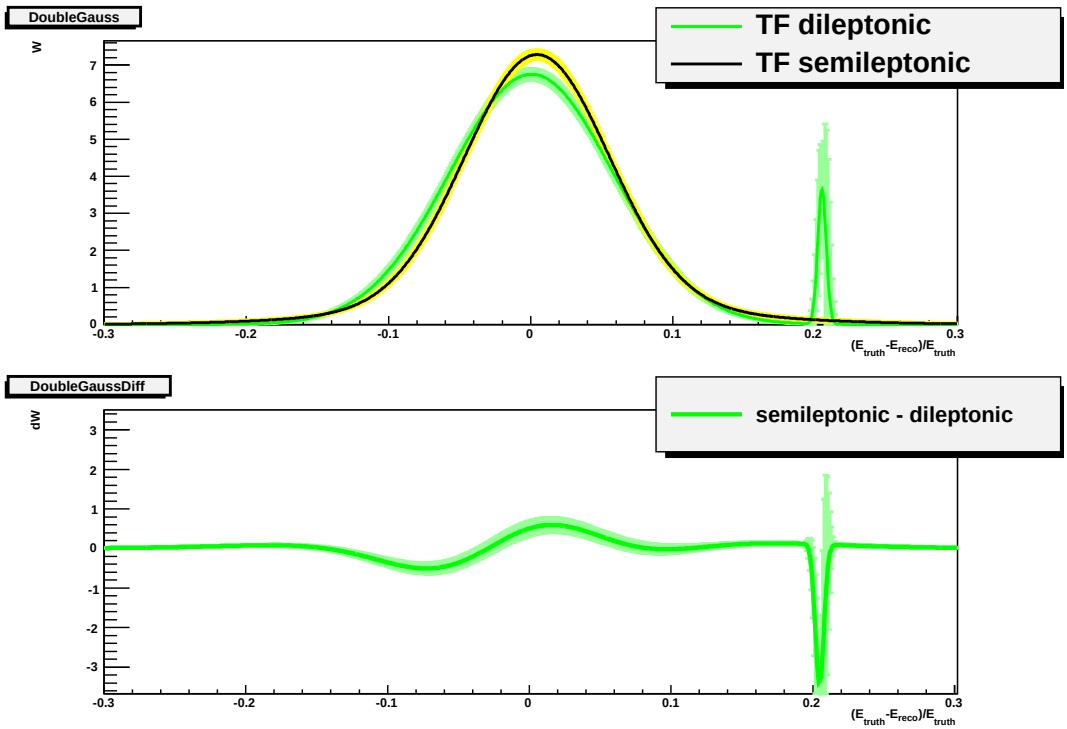

Figure 5.42: Transfer functions for MC10b muons in the $|\eta|$ region $|\eta| \in [1.11; 1.25]$ at 100 GeV.

5.7 B-tag

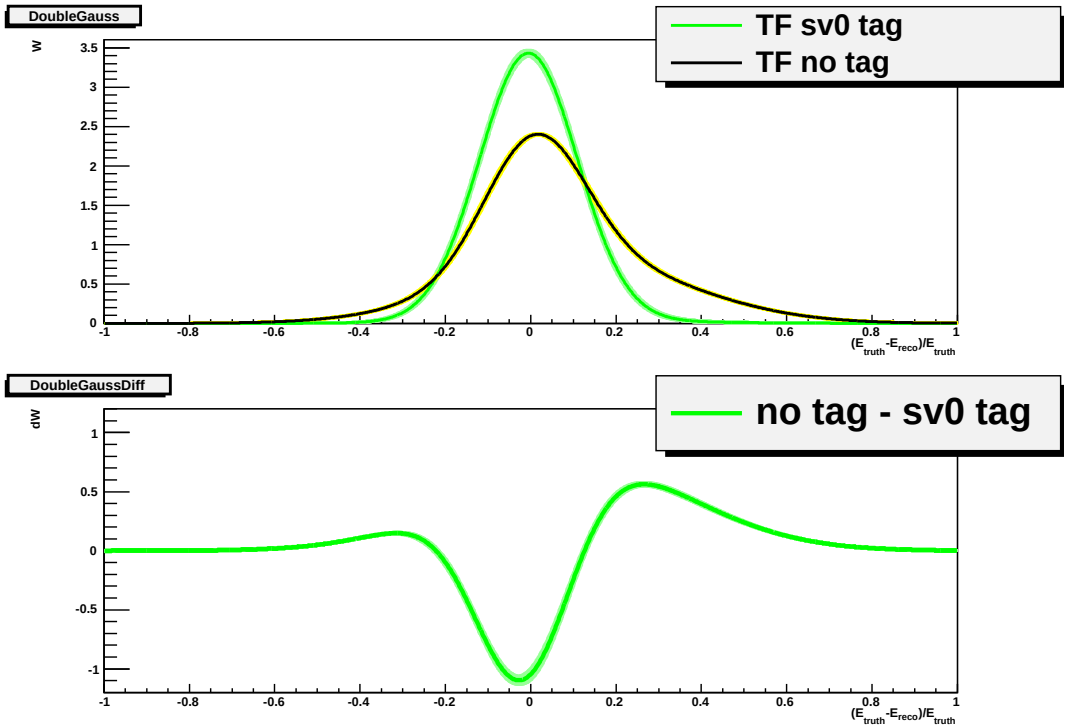

Figure 5.43: Transfer functions for MC10b b-jets in the $|\eta|$ region $|\eta| \in [0; 0.8]$ at 100 GeV.

The figures 5.43, 5.44 and 5.45 show the comparision of transfer functions with and without the svo lifetime tag. The transfer functions with the tag have a smaller width and have lower energy losses.

To ensure this effect is not a result of a bad fit the transfer functions have been compared to the histograms created by TFTool. This is shown for the $|\eta|$ region from 0.00 to 0.80 in the figures 5.46, 5.47, 5.48 and 5.49. The comparision shows, that this effect is visible not only in the transfer functions but also the data.

This effect is clearly visible in the fits to the scale of the second Gauss. This is shown in figure 5.50. For the transfer function with the sv0 tag the scale is much smaller.
This effect results from the lifetime tag. Lifetime tagged b-jets have a different ratio of charged to neutral particles they decay into than no tagged b-jets. This ratio is higher for tagged b-jets. Since calorimeter response is better for charged particles this leads to lower energy losses and thus to a narrower transfer function.
These results show, that transfer functions for not tagged b-jets must not be used for reconstruction of tagged b-jets and vice versa. It is necessary to calculate separate transfer

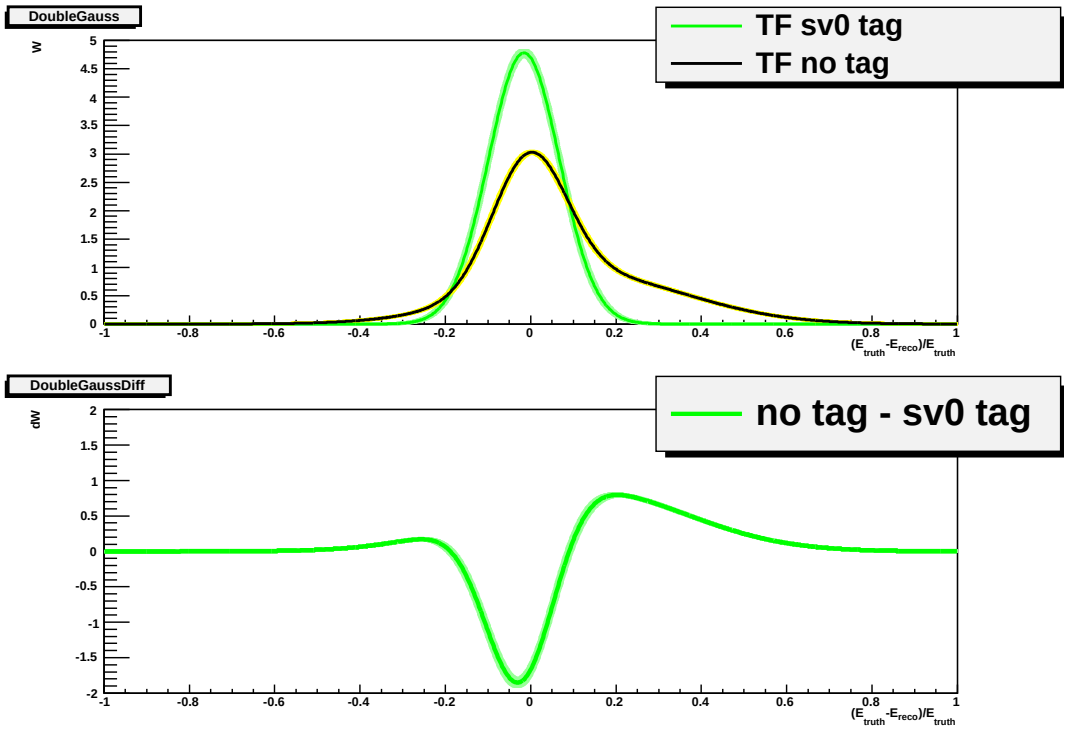

Figure 5.44: Transfer functions for MC10b b-jets in the $|\eta|$ region $|\eta| \in [0; 0.8]$ at 250 GeV.

functions for lifetime tagged b-jets and not tagged b-jets.

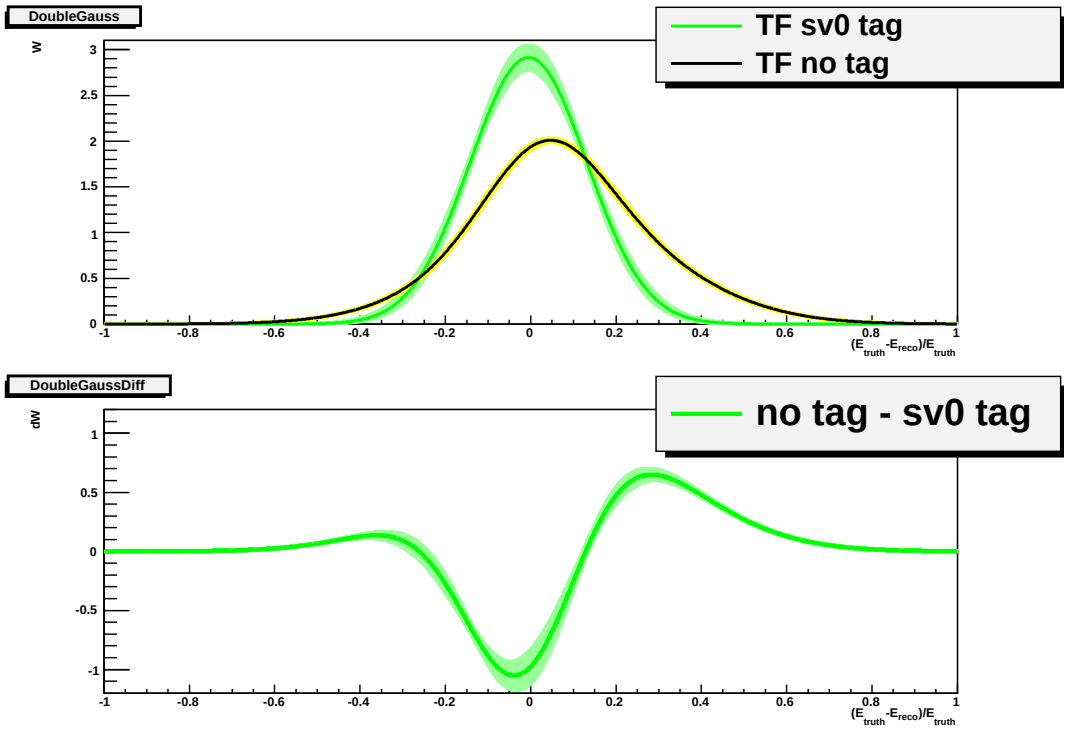

Figure 5.45: Transfer functions for MC10b b-jets in the $|\eta|$ region $|\eta| \in [1.52; 2.5]$ at 100 GeV.

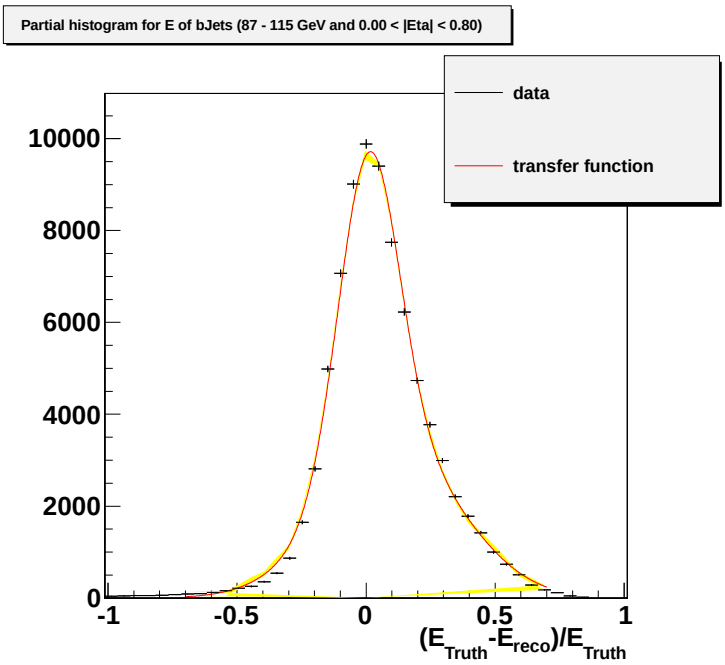

Figure 5.46: Transfer function for MC10b b-jets without sv0 tag in the $|\eta|$ region $|\eta| \in [0; 0.8]$ at 101 GeV compared to data.

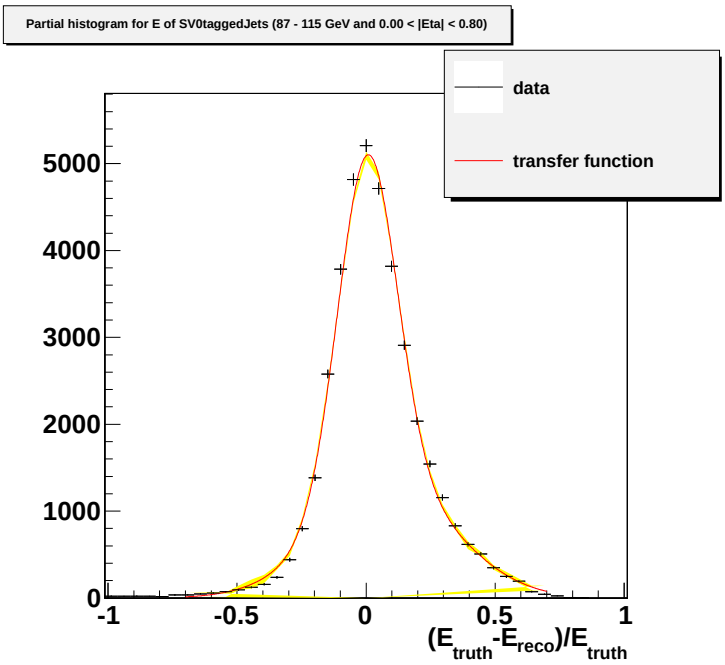

Figure 5.47: Transfer function for MC10b b-jets with sv0 tag in the $|\eta|$ region $|\eta| \in [0; 0.8]$ at 101 GeV compared to data.

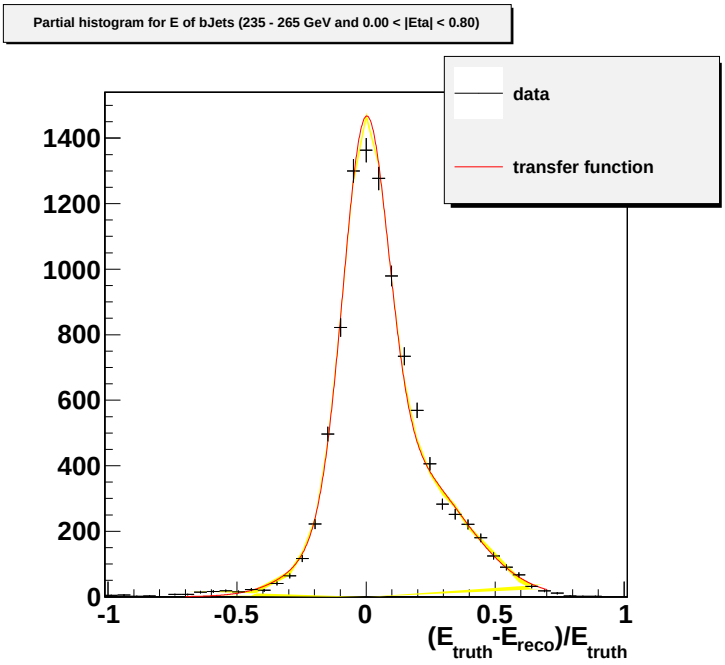

Figure 5.48: Transfer function for MC10b b-jets without sv0 tag in the $|\eta|$ region $|\eta| \in [0; 0.8]$ at 250 GeV compared to data.

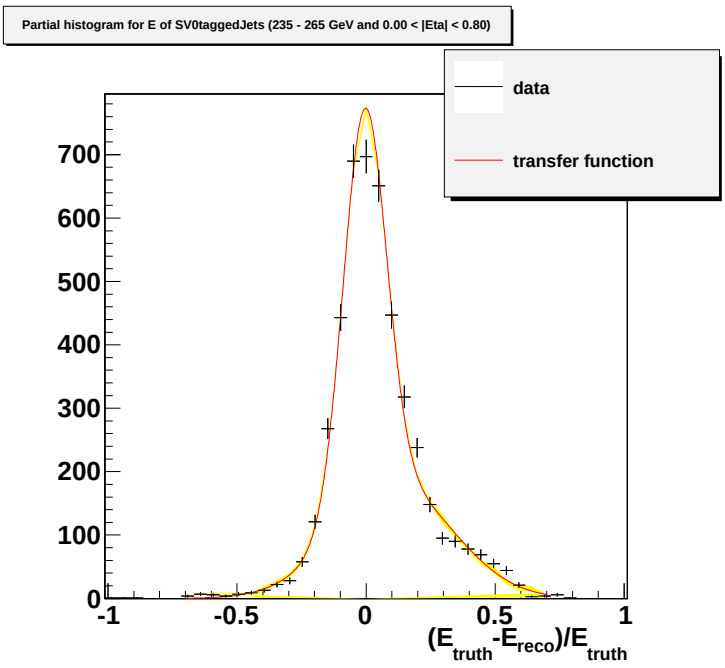

Figure 5.49: Transfer function for MC10b b-jets with sv0 tag in the $|\eta|$ region $|\eta| \in [0; 0.8]$ at 250 GeV compared to data.

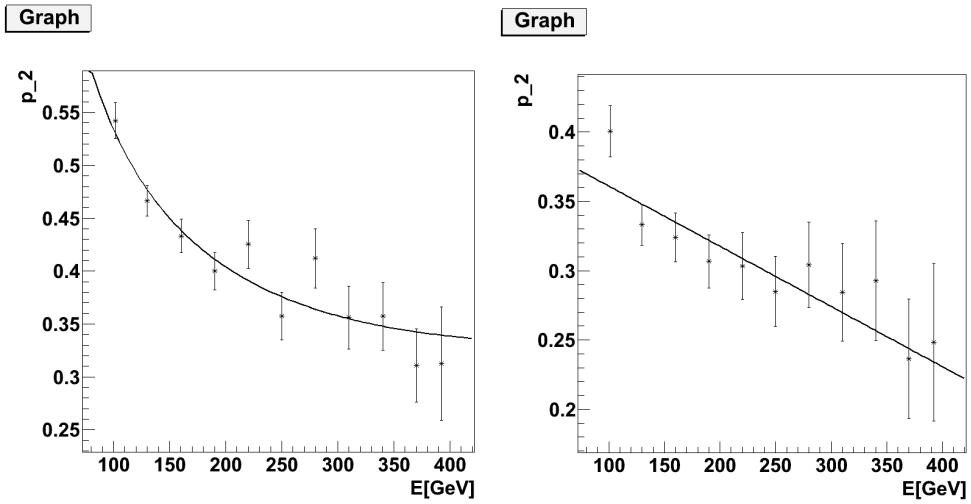

Figure 5.50: Fit to the parameter scale(p_2) for MC10b b-jets in the $|\eta|$ region $|\eta| \in [0; 0.8]$. Shown on the left side is the fit without the tag and on the right side with the sv0 tag.

6 Conclusion

In this bachelor thesis the systematic uncertainties of transfer functions used by KLFitter have been investigated. In order to do this a variety of parameters were changed one by one and different MC samples have been used. The transfer functions created with these new parameters and MC samples were then compared to the ones with unchanged parameters.

First the influence of lowering the lower end of the energy fit range was investigated. This change yielded litte effect on the transfer functions themselves but increased their uncertainties because the low energy parameters from the local fit tend to be far off the functions fitted to the high energy parameters.

The second investigated parameter was the matching radius. The matching radii $dR = 0.30$, $dR = 0.10$ and $dR = 0.05$ have been tested. Lower matching radii resulted in a transfer function shifted to lower values of $\frac{E_{truth}-E_{reco}}{E_{truth}}$.

MC samples with different top quark mass assumptions (160 $\frac{\text{GeV}}{c^2}$, 175 $\frac{\text{GeV}}{c^2}$ and 190 $\frac{\text{GeV}}{c^2}$) have been used to create transfer functions. Their effect on the transfer function was negligible because they only change the kinematics of the event not the pileup and other effects that have an influence on the transfer function. This allows merging these samples to increase statistics.

After this it was tested which influence the correlations between the parameters of the transfer functions have on the uncertainties. The effect was not negligible and thus the correlations have to be taken into account when using the uncertainties of the transfer functions for an analysis.

The fifth test was changing the maximum number of jets allowed in an event. This yielded a shift of the transfer functions to higher values of $\frac{E_{truth}-E_{reco}}{E_{truth}}$ because small jets from the underlying event were missing and thus not merged into the jets from the $\bar{\text{t}}\text{t}$ decay.

Then the difference between transfer functions for the semileptonic decay channel and the dileptonic decay channel has been investigated. The difference was small und compatible with zero within its uncertainties for electrons. Thus these samples can be merged when calculating electron transfer functions in the future to increase statistics.

The last tested effect was the influence of a sv0 lifetime tag for b-jets. The transfer function

created using the tag differed significantly from the ones without the tag. This resulted from the changed charged to neutral particle ratio in the decay of the tagged b-jets which leads to better calorimeter response und thus less energy loss. Because this difference is far from being negligible, separate transfer functions for tagged and not tagged b-jets have to be used.

Bibliography

[1] CDF Collaboration, Observation of the Top Quark, Phys.Rev.Lett. 74, 2626-2631 (1995)

[2] D0 Collaboration, Observation of the Top Quark, Phys.Rev.Lett. 74, 2632-2637 (1995)

[3] K. Nakamura et al. (Particle Data Group), Review of Particle Physics, J. Phys. G 37, 075021 (2010)

[4] P. Nason, S. Dawson, R.K. Ellis, The Total Cross Section for the Production of Heavy Quarks in Hadronic Collisions, Nucl. Phys. B 303, 607 (1988)

[5] D0 Collaboration, Multivariate searches for single top quark production with the D0 detector, Phys. Rev. D 75 (2007)

[6] ATLAS Collaboration, The ATLAS Experiment at the CERN Large Hadron Collider, Journal of Instrumentation 3, S08003 (2008)

[7] L. Evans, P. Bryant, LHC Machine, Journal of Instrumentation 3, S08001, http://stacks.iop.org/1748-0221/3/i=08/a=S08001 (2008)

[8] J. Erdmann, K. Kroeninger, O. Nackenhorst, A. Quadt, Kinematic fitting of ttbar-events using a likelihood approach: The KLFitter package, ATLAS Note ATL-COM-PHYS-2009-551, CERN, Geneva (2009)

Acknowledgement

I would like to thank Prof. Dr. Arnuf Quadt for giving me the opportunity to write my Bachelor Thesis in the field of particle physics, for being the first referee and for his great letures which fostered my interest in particle physics. I would also like to thank Prof. Dr. Johannes Haller for being the second referee. Additionally I would like to thank Prof. Dr. Ariane Frey for her great lectures in particle physics.
Sincere thanks to Dr. Kevin Kröninger for supervising my work. Especially I would like to thank Dipl. Phys. Boris Lemmer for supervising my work, the assistance he gave me along the way and the time he invested. Without his help this thesis would not have become what it is.

Erklärung nach §13(8) der Prüfungsordnung für den Bachelor-Studiengang Physik und den Master-Studiengang Physik an der Universität Göttingen:

Hiermit erkläre ich, dass ich diese Abschlussarbeit selbständig verfasst habe, keine anderen als die angegebenen Quellen und Hilfsmittel benutzt habe und alle Stellen, die wörtlich oder sinngemäß aus veröffentlichten Schriften entnommen wurden, als solche kenntlich gemacht habe.
Darüberhinaus erkläre ich, dass diese Abschlussarbeit nicht, auch nicht auszugsweise, im Rahmen einer nichtbestandenen Prüfung an dieser oder einer anderen Hochschule eingereicht wurde.

Göttingen, den May 31, 2012

(Fritz Pasternok)